Sensors & Diagnostics

TUTORIAL REVIEW

View Article Online
View Journal

Cite this: DOI: 10.1039/d5sd00186b

Recognition of illicit date rape drugs: a luminescence sensing perspective

Sunita Kyndait, Trisha Das, Dikshit Bokotial and Aniket Chowdhury *

The consumption of recreational and addictive substances has rapidly increased owing to the legalisation of cannabinoids and the emergence of new potent synthetic psychoactive substances such as stimulants, depressants, and opioids. Moreover, due to lucrative financial aspects, the cooperation between international organised criminal syndicates has led to a surge in the worldwide distribution of narcotics. The use of darknet, encrypted software, and untraceable communication has also complicated the detection and confiscation of the drugs. Although the major attention of the law enforcement has been directed towards addictive substances, the non-lethal party drugs or illicit date rape drugs have gradually emerged, which could induce long-term psychological and physical trauma on the victim. Several heavy instrument-based and portable devices are now commercially available for their detection, which rely on various spectroscopic and spectrometric principles. The use of luminescent molecules in this regard proves beneficial due to their portability, sensitivity, selectivity, and, most importantly, sensing capacity even in clandestine environments. Although several literature reports are available on the sensing of illicit narcotics encompassing all types of psychoactive drugs, such as opioids, cathinones, cannabinoids, and synthetics, a comprehensive exploration of illicit date rape drugs remains elusive. Therefore, in this perspective, an attempt is made to comprehensively evaluate all types of luminescent sensors, which are reported for the detection of illicit date rape drugs, including GHB, benzodiazepines and ketamine.

Received 21st October 2025,
Accepted 16th January 2026

DOI: 10.1039/d5sd00186b

rsc.li/sensors

1. Introduction

The rapidly growing abuse of narcotics among the global young population is posing a serious concern. As per the "World Drug Report 2025" published by the "United Nations Office on Drugs and Crime", 316 million people, comprising roughly 6% of the young and middle-aged population of the world, were engaged in drug abuse in 2023 alone, excluding the alcoholics and tobacco users from the statistical analysis.[1]

The adverse effects of controlled substance usage range from addiction, paranoia, poor mental health, and aggression to more severe problems such as liver and kidney damage, cardiac arrest, and even death from unsupervised

Department of Industrial Chemistry, School of Physical Sciences, Mizoram University, Tanhril, Aizawl-796004, Mizoram, India.
E-mail: aniketmzu@gmail.com, mzut239@mzu.edu.in

Sunita Kyndait

Sunita Kyndait has completed her MSc in Industrial Chemistry from the Department of Industrial Chemistry, Mizoram University, in 2024. Subsequently, she joined the same department as a graduate student under the guidance of Dr. Aniket Chowdhury. Her work is mainly focussed on the development of luminescent donor–acceptor type small molecules for sensing applications.

Trisha Das

Trisha Das has completed her MSc in Industrial Chemistry from the Department of Industrial Chemistry, Mizoram University in 2022. Subsequently, she joined the same department as graduate student under the guidance of Dr Aniket Chowdhury. Her main work is in the field of luminescent triphenylamine-based twisted systems for artificial light harvesting.

overconsumption.[2] Around half a million people have lost their lives to drug abuse in 2023 alone.

The illicit drugs encompass a large category of different natural and synthetic organic molecules that are procured illegally and used for recreational purposes. According to the USFDA, these illicit drugs are also termed "drugs of abuse" as they are used in a frequency or quantity often surpassing the medically recommended dose.[3] Moreover, the distribution of these drugs is strictly regulated following the guidelines of "The Single Convention on Narcotic Drugs, 1961" and "Convention on Psychotropic Substances, 1971", which led to the coinage of the term "controlled substances".[4,5]

Following the historical evidence, the recreational use of natural substances can be traced back to various ancient civilisations in different timelines throughout the world. Mainly, plant-derived extracts such as cocaine, cannabis, and opium were used by Aztecs, Indians, and Mediterranean civilisations.[6–8] Later, pharmaceutical analogues such as oxycodone, hydrocodone, and benzodiazepines gained notoriety. The desire to prolong the pharmacological effect of the drugs led to the development of more potent "designer drugs" such as amphetamines and methylenedioxy amphetamines.[9] To circumvent the regulatory authorities, the existing illicit drugs are often structurally modified to afford "new psychoactive substances", which are the latest addition to the long list of narcotics.

The increasing demand for different types of recreational and addictive substances has led to a surge in the illegal trafficking of narcotics in different parts of the world. As per the "European Drug Report 2024", published by the "European Monitoring Centre for Drugs and Drug Addiction", the number of various drugs seized only in the EU has skyrocketed in the last decade, including cocaine (+376%) and methamphetamine (+293%).[10] The drug money is also known to fuel regional instability in places like Myanmar, Colombia, Venezuela, and Mexico, which led to the coinage of the term "Narco-terrorism".

The street available illicit drugs are broadly categorised into four segments, which are depressants, stimulants, opioids, and hallucinogens. Almost all of them interact with the central nervous system with a particular focus on the serotonin and dopamine receptors, which are responsible for locomotion and brain function.[11] On the one hand, depressants, also commonly known as "Downer" such as alcohol, benzodiazepines, and cannabis, obstruct the neurotransmission, leading to a relaxed sensation. The stimulants or "Uppers", on the other hand, accelerate the brain activity, ultimately culminating in a higher degree of alertness and enhanced stamina.[12] Unfortunately, the overdose of stimulants such as cocaine and amphetamine often led to a panicky or frenzied situation and untimely death due to cardiac arrest or cerebral stroke from excessive blood circulation. The opioids such as morphine, codeine, and heroin are mostly used as pain relievers, and the hallucinogens such as LSD and magic mushroom bring the user into a euphoric state.

The recreational use of illicit drugs directly affects the brain's reward system, and such abuse leads to a wide array of mild and severe consequences such as addiction, fatigue, weight loss, mood swing, anger management, and tendency to commit violent crime, traffic accidents, spread of infectious disease, *etc.*[13] The accidental overdose of opioids can even deplete oxygen intake, due to which vital organs like the heart or brain stop functioning, leading to sudden death. To tackle such issues, the law enforcement officers as well as first responders are equipped with various drug detection kits as well as opioid antidotes such as Narcan.[14] Although the aforementioned incidents constitute the majority of the financial and societal burden of drug abuse, the drug-associated crimes are also a major concern. Among the different drug-related crimes, such as vandalism, theft, homicide, and traffic violation, the drug-facilitated sexual assault (DFSA) is of particular concern. Statistical analysis reflected that about 15–20% of the sexual assault cases

Dikshit Bokotial

Dikshit Bokotial has completed his MSc in Industrial Chemistry from the Department of Industrial Chemistry in 2021, Mizoram University. Subsequently, he joined the same department as a graduate student under the guidance of Dr Aniket Chowdhury.

Aniket Chowdhury

Dr Aniket Chowdhury completed his Master's degree in Chemistry from the Indian Institute of Technology Kharagpur in 2011. He joined the Indian Institute of Science (Bangalore) in Prof. Partha S. Mukherjee's research group and obtained his PhD in 2017, working on discrete 2D and 3D organic and metal–organic architectures. Currently, he is working as an Assistant Professor at the Department of Industrial Chemistry, Mizoram University. His research interest involves artificial light harvesting and luminescent materials.

against women are induced by unwilling ingestion of drugs by drink spiking, and the outcome of such assault cases ranges from molestation, rape, as well as accidental death from overdose, ultimately culminating in profound physical and psychological impact on the victim. The DFSA drugs are mostly categorised as follows: i) GHB class [gamma hydroxy butyric acid (GHB), gamma-butyrolactone (GBL), gamma-valerolactone (GVL), sodium oxybate (Na-GHB), and 1,4-butane diol (1,4-BD)]; ii) benzodiazepines [flunitrazepam (Rohypnol), diazepam (Valium), chlorodiazepam (Librium), clonazepam (Klonopin), alprazolam (Xanax), lorazepam (Ativan), and nimetazepam (Lavol)]; iii) alcohol, and iv) ketamine.[15] The detection of these drugs which are also known as date rape drugs is particularly difficult due to the following facts: i) these drugs are highly soluble in water and ethanol, and are both colourless and odourless and ii) their fast metabolism makes, the detection of these drugs in body fluids such as urine and blood very complicated, which led to the classification of GHB drug as Schedule I drug as per the USDAs' Hillory J. Farias and Samantha Reid Date-Rape Prevention Act of 2000.[16]

Therefore, the detection kits of illicit drugs used in DFSAs require special attributes such as rapidity, reliability, reproducibility, selectivity and most importantly sensitivity. Different major and minor instrumental techniques have been formulated for the on-field detection of narcotics, and some of the key equipment are independent and combined chromatography-mass spectrometry (GC–MS, LC–MS, HPLC-MS, and ESI-MS), ion-mobility, electrophoresis, NMR, SERS, X-ray backscattering, electrochemical detectors (potentiometric sensors, field-effect transistors, three-electrode sensors, and potentiometric sensors), immunosensors, *etc.*[17] Unfortunately, due to massive size, high energy consumption, and complicated time-consuming installation, the use of aforementioned equipment is mostly limited to large places with high passenger volume, such as airport, train stations or any other international border. More compact and easier-to-use alternatives such as portable Raman or trained canines are being used by the police forces for the mobile detection of narcotics.[17] The Raman spectrometer requires time-consuming sample preparation as well as a large comparison database and the canines often experience work fatigue, require long training hours and are susceptible to drug overdose. In this regard, the chromogenic and fluorogenic detection kits appear to be suitable alternatives as they are easy to manufacture, extremely light, and easily disposable and provide immediate results. The fluorogenic sensors, in some aspects, appear even superior to the chromogenic counterparts as the latter often requires multiple attempts for accuracy, leading to higher risks of drug exposure. Another key advantage of the fluorogenic probes is that they can be used by people suffering from colour blindness and poor eyesight in places with low lighting and most vulnerable to drink spiking, such as nightclubs, rave parties, bars, dark alleyways, streets, and clandestine labs.

This perspective summarises the various fluorogenic probes that are both commercially available and used by law enforcement officers for the detection of illicit date rape drugs. Previously, several manuscripts have incorporated comprehensive reviews on different types of sensors for illicit drugs, and they were mostly focused on either the sensing methodology, such as optical sensing, biomaterial sensing, nano material-based sensing, and sensing of drugs in the body fluids, water, cannabinoids or opioids.[18–23] Several reports that encompass all the available detection methods have also emerged, but they are either target-specific, such as GHB or too general by incorporating all illicit drugs.[24–29] Therefore, a concise report on luminescent sensors of illicit date rape drugs was due, and in this manuscript, an attempt has been made to fill the much-needed void by using a complete analysis of luminescent sensors of date rape drugs, which is anticipated to provide a much-desired reference for future research.

2. Mechanistic investigations of fluorescent sensors for date rape drugs

The luminescence-based sensing of any sensor-analyte combination depends on two key factors: the mechanism of interaction between the sensor and analyte and the effect of the interaction on the sensor emission. In a previous review, Shaw, Chen, and Burn elaborated on the different interaction pathways in which energy transfer or electron migration occurs between the sensor and the analyte.[12] Therefore, in this report, the numerous outcomes are explained in detail.

The different types of sensor-analyte interactions result in three types of emission responses from the fluorophore, which are i) emission quenching, ii) emission enhancement, and iii) emission switching.[30,31] They are elaborated herein.

2.1. Quenching of fluorescence of the sensor

The primary response observed for the majority of the fluorescent sensors is the quenching of the emission after the addition of analytes. A detailed mechanistic investigation established a wide variety of pathways *via* which the emission of a fluorophore can be dissipated *via* non-emissive processes, which are listed below (Scheme 1).

2.1.1. Heavy atom-induced quenching. Upon photoirradiation, the excited fluorophore moves around in the solution, and when it encounters a paramagnetic sample, such as oxygen or a heavy atom, such as iodine it can transfer the energy to the non-emissive excited triplet state of the other atom or molecule, leading to a drastic drop in singlet population, as observed in Fig. 1. This can occur upon collision between the fluorophore and the heavy atom (Scheme 1). The loss of the singlet population of the fluorophore reflects in the quenching of the emission, and this phenomenon is termed paramagnetic quenching.[32]

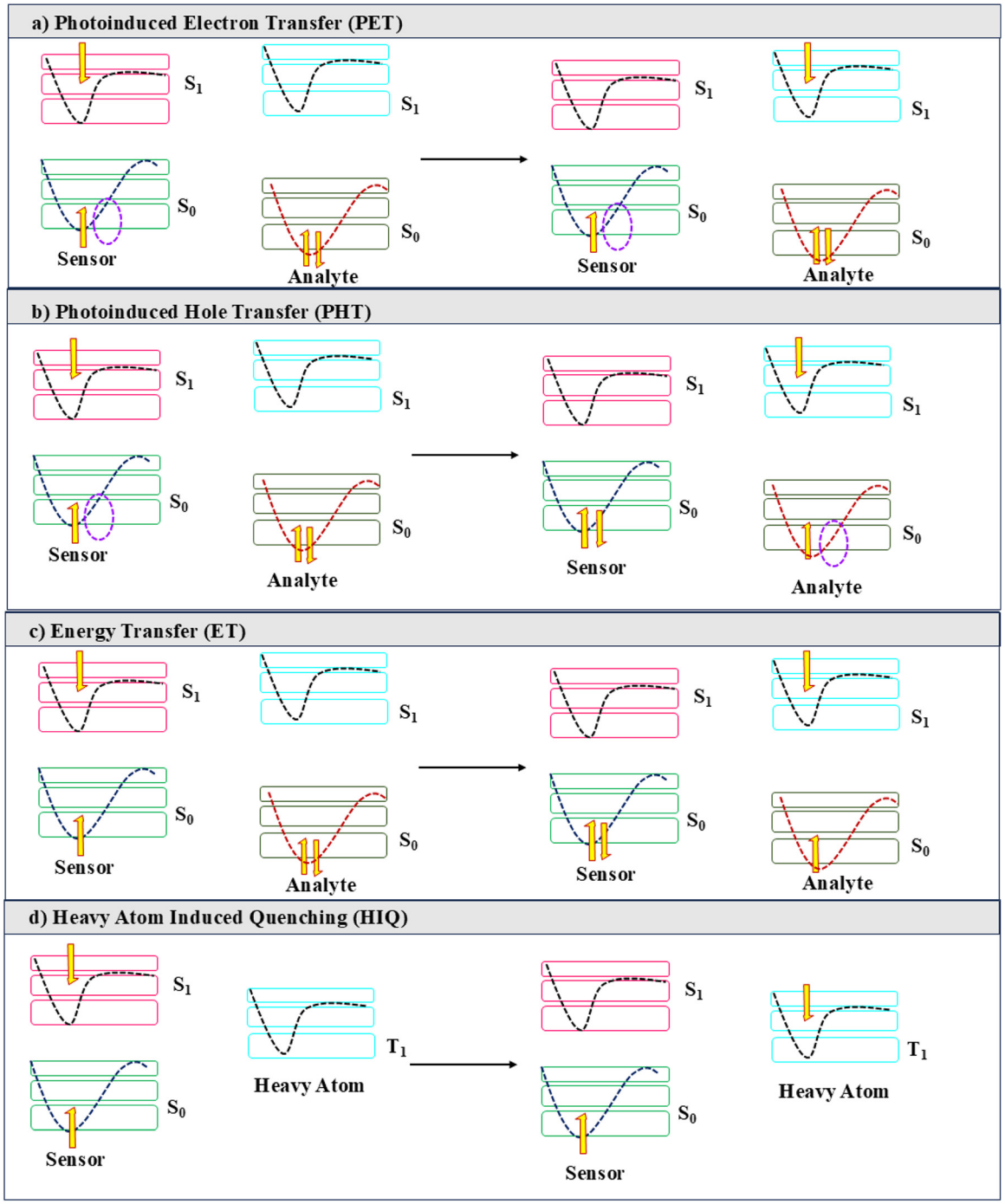

Scheme 1 Different mechanisms for emission quenching: a) photoinduced electron transfer, b) photoinduced hole transfer, c) energy transfer, and d) heavy atom-induced quenching.

2.1.2. Excimer and exciplex formation. It is mostly observed for polyaromatic samples which are susceptible to arrange themselves into close proximity utilising π–π interactions. Under normal excitation conditions, a single molecule absorbs energy and releases it *via* luminescence. However, in the case of dimeric systems, upon excitation, one such excited fluorophore can transfer its energy to the neighbouring molecule in the ground state, leading to the loss of monomer emission (Fig. 1). The bimolecular composite furnishes a red-shifted emission called excimer emission and the fluorophore pair is called excimer. When two fluorophores are substituted with a sensor-analyte association complex, this closely oriented system is called an exciplex, which can also lose excited-state energy *via* non-radiative decay.[33]

2.1.3. Photoinduced excited-state processes. The photoinduced excited-state processes involve mainly electron, hole and proton transfer phenomena. The UV-induced

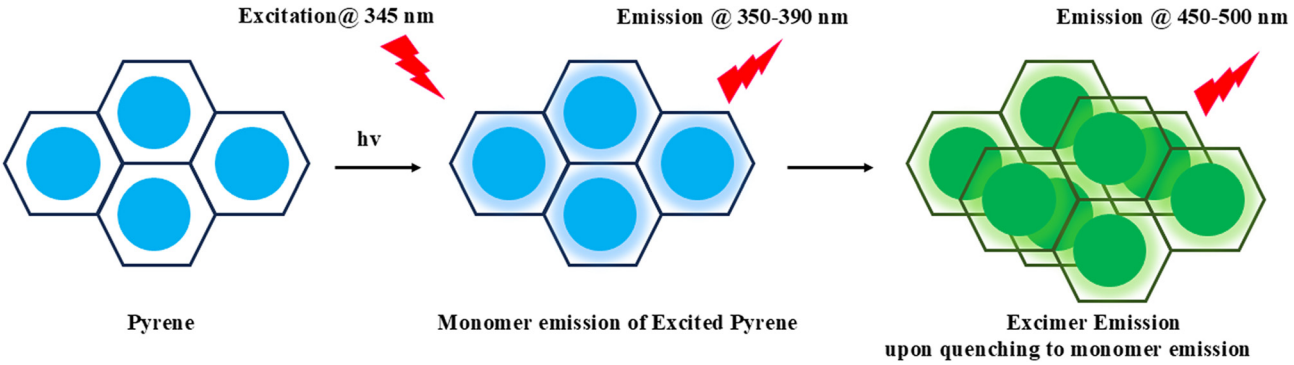

Fig. 1 Excimer formation-induced emission quenching of pyrene.

excitation of the fluorescent sensor initiates all these types of energy loss pathways explained below.

2.1.3.1. Photo-induced electron transfer. After photoirradiation, the excited electron migrates from the S_1 state of the excited fluorophore to the S_1 state of the analyte in the ground state, as observed in Scheme 1. Due to such non-radiative decay of the excited-state energy, luminescence is quenched. The analyte being non-fluorescent releases energy *via* a non-radiative pathway and the excited electron returns to the S_0 state of the sensor, leading to photo-induced electron transfer.[17]

2.1.3.2. Photo-induced hole transfer. In this process, a hole or vacancy is generated in the sensor after an electron gets excited from S_0 to S_1 of the luminescent sensor upon UV irradiation. Subsequently, the hole is filled by transporting an electron from the S_0 state of the analyte and to the S_0 state of the sensor (Scheme 1). Thus, any kind of radiative relaxation of the excited-state electron becomes restricted, and it migrates to the S_1 state of the non-luminescent analyte. Such type of emission loss is known as photo-induced hole transfer.[17]

2.1.3.3. Photo-induced proton transfer. When the sensor has multiple possible configurations, the photoexcitation initiates the exchange of the protons to facilitate the tautomerisation into a non-emissive but stable configuration of the sensor.[34]

2.1.4. Energy transfer. The excited-state energy can also be transferred through space between the sensor and the analyte, which often results in emission decay. In this process, the exchanged energy is utilised to migrate an electron from the ground to the excited state of the analyte, and being non-fluorescent, the excitation energy is released *via* a non-emissive pathway (Scheme 2).

2.1.4.1. Forster resonance energy transfer. When the emission of the sensor and the absorption of the analyte overlap, and the entities are substantially away from each

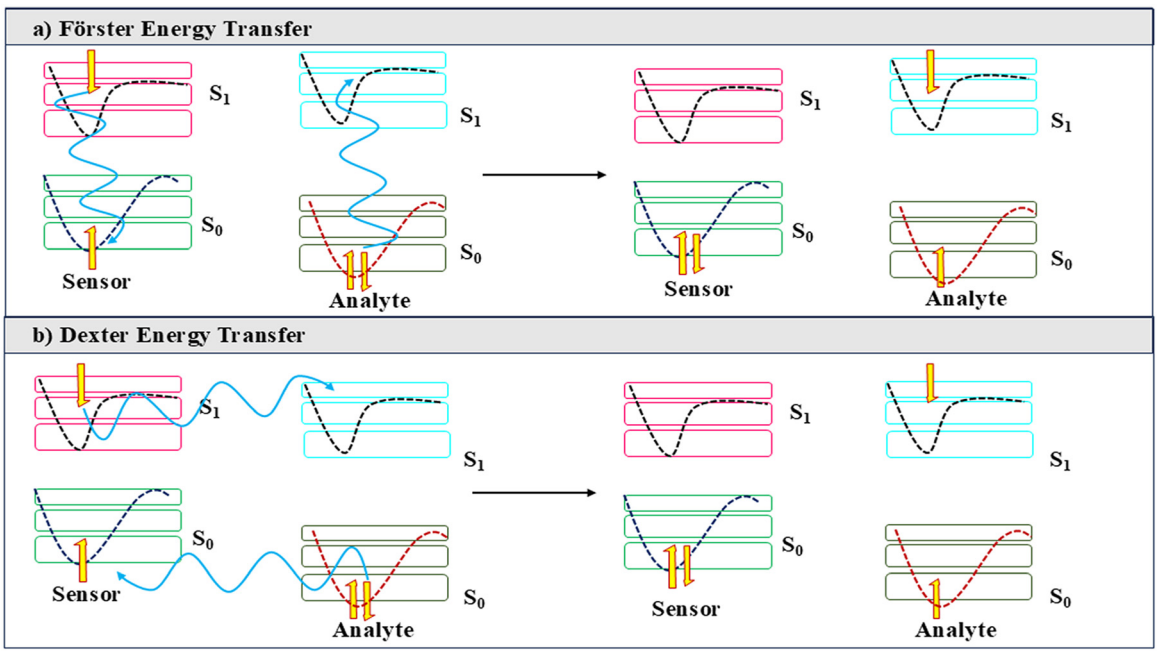

Scheme 2 Different energy transfer pathways for quenching, (a) Forster Energy Transfer, and (b) Dexter Energy Transfer.

other, the energy migrates through space, leading to fluorescence quenching (Scheme 2).[17]

2.1.4.2. Dexter energy transfer. When the sensor and the analyte are in very close proximity, the excited-state energy migrates through space directly from the excited sensor to the analyte, resulting in emission quenching (Scheme 2).

2.2. Fluorescence enhancement

The fluorescence quenching leads to loss of emission intensity *via* a wide range of mechanisms explained above. However, the emission quenching suffers from several drawbacks, which are background interference, poor signal-to-noise ratio, high LOD, self-quenching of the sensor, *etc.* To mitigate these drawbacks, scientists have developed a new generation of sensors; these sensors are normally non-emissive in nature, but once an analyte is added, a sharp fluorescence enhancement is observed.

The emission enhancement mainly occurs *via* negation of any of the aforementioned mechanisms, which initially hinder the radiative decay from the sensor.

2.2.1. Conventional fluorescence enhancement. The conventional fluorescence enhancement occurs when the sensor initially loses excited state energy *via* any of the non-radiative pathways elaborated before. The binding of the analyte leads to the elimination of such pathways and the energy is released in the form of fluorescence.

2.2.2. Emission enhancement *via* chemical reactions. Sensor–analyte interactions occur several times *via* chemical reactions, leading to the creation of luminescent species by the fragmentation of either the sensor or the analyte, leading to the appearance of an emission peak.

2.2.3. Aggregation-induced emission. It is a new phenomenon, in which the binding of the analyte leads to the structural rigidification of the sensor, followed by a restrictive energy loss *via* any type of non-radiative pathways, such as molecular rotation or vibration, leading to emission enhancement. As observed in Fig. 2b, the emission of sensor **3** in its free form was negligible due to excitation energy loss mediated by nonradiative decay, such as aromatic ring rotation and vibration. Once Zn^{2+} was added, a more structurally rigid complex was generated, which led to emission enhancement.[35]

2.3. Ratiometric sensor

Although fluorescence enhancement removes the background signals, the accurate determination of the saturation point is cumbersome, which often leads to errors in the LOD estimation. The ratiometric sensor, where a new peak is generated at the expense of the initial emission, is the most accurate as it compares the peak intensity ratio with the analyte concentration, leading to a more accurate result. From Fig. 2a, it is evident that sensor **1** furnished an emission maximum at 475 nm. In the presence of an incremental amount of Hg^{2+}, the sensor hydrolysed into compound **2** with a new emission at 550 nm, highlighting a strong ratiometric response (Table 1).[36]

3. Fluorescent detectors for GHB class of illicit date rape drugs

Literature survey revealed that a wide variety of luminescent systems, ranging from organic small molecules, metal complexes, synthetic polymers, biomolecules, supramolecular architectures such as COF, MOF, and SCCs, to organic and inorganic nanomaterials, have been employed to develop different types of sensors for illicit drugs.[18–29] In this perspective, the main attention is directed to luminescent systems, which are fabricated to specifically target illicit date rape drugs of GHB origin.

3.1. Organic small molecule-based fluorescent sensors

The GHB class of drugs mainly constitute three primary drugs, which are gamma-hydroxybutyric acid (GHB), its cyclised precursor gamma-butyrolactone (GBL), and the analogous gamma-valerolactone (GVL). Apart from that, the corresponding sodium salts of GHB sodium oxybate (Na-

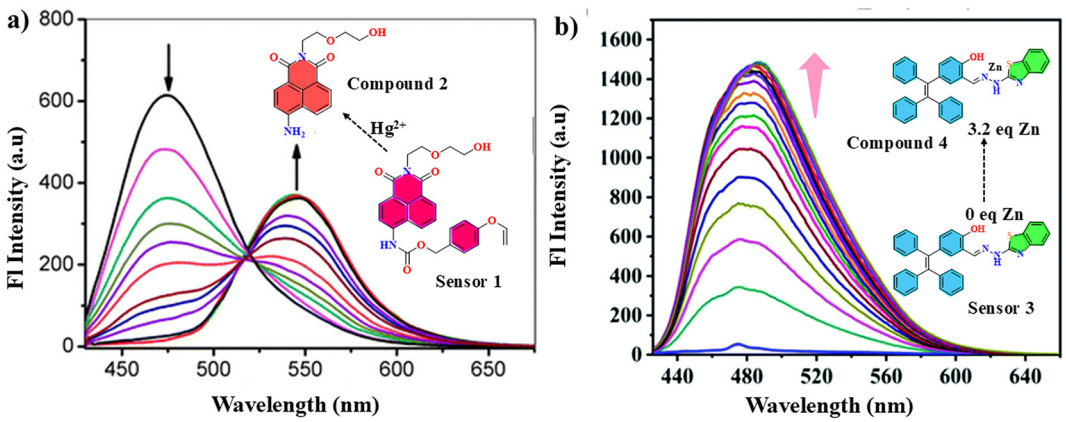

Fig. 2 a) Ratiometric sensing and b) emission enhancement *via* the AIE pathway. Reprinted with permission from ref. 35 and 36. Copyright 1996 and 1987, the Royal Society of Chemistry.

Table 1 Summary of different luminogenic probes for detecting submission drugs

System	Analyte	Sensing mechanism	Sensing medium	LOD	Limitation	Ref.
Organic small-molecule (BODIPY, "Green Date")	GBL	GBL-induced disassembly of non-emissive aggregates leading to fluorescence turn-on	Water, alcoholic & non-alcoholic drinks (≤10% EtOH)	34.88 mM	Performance decreases at high alcohol content; limited selectivity	38
Organic small-molecule (modified BODIPY, "GHB Orange")	GHB	Hydrogen-bond-assisted PET causing fluorescence quenching	Alcoholic beverages (up to 50% solvent)	~96.05 mM	Interference from other carboxylic acids and drugs	39
Organic small-molecule (hydrazone-/benzothiazole-BODIPY)	Na-GHB; synthetic cathinones	GHB-induced spectral shift; Cu(II)/Cu(I) redox for cathinones	Soft drinks	0.3–0.4 μM (GHB); ~2 μM (SCs)	Multi-step sensing; metal-ion dependence	40
Organic small-molecule (naphthoxazole/fluorescein derivatives)	GHB	GHB-induced deprotonation causing ratiometric absorbance and fluorescence turn-on	Alcoholic beverages	0.12 μM	Requires organic solvent (DMSO); limited aqueous performance	41
Paper-strip organic sensor (fluorescein-decorated naphthoxazole/benzoxazole)	GHB	Fluorescence enhancement or ratiometric response on cellulose	Drinks (solid-state strips)	0.06–0.45 μM	Sensitivity insufficient for biological fluids	42
Organic small-molecule (HBT-based ESIPT probes)	GHB	Hydrogen bonding and keto–enol tautomerism (ESIPT modulation)	Solution	5.62 nM (fluorescence); 660.87 nM (colorimetric)	Limited validation in real beverages	43
AIE-active organic probes (fluorene–cyanostilbene)	GHB	H-bond-induced aggregation changes with ratiometric fluorescence	Dioxane–water; paper strips	~5 mM	High detection concentration; alcohol dependence	44
Metal complex (Ir(III) phosphorescent probe)	GHB	GHB-induced excited-state perturbation causing phosphorescence quenching	Drinks, milk	1.44 mM	Requires UV source and instrumentation	48
Metal complex (Fe^{3+}–BODIPY indicator displacement)	GHB	GHB displaces ligand from Fe^{3+} restoring fluorescence	Drinks; paper strips	2.40 mM	Strip stability and metal-salt shelf-life issues.	49
Metal complex (Cu^{2+}–coumarin displacement)	GHB	Preferential Cu^{2+} binding by GHB releases fluorescent coumarin	Diluted beverages; paper strips	0.03 μM (buffer); 0.1 μM (drinks)	Requires dilution; metal-based formulation	50
Nanomaterial (dye-functionalized silica nanoparticles)	GHB	Surface-induced chromogenic/fluorogenic response	Solution; cellulose paper	1.65–96 mM	Reduced sensitivity upon immobilization	51
Ionic-liquid-based nanoparticles (fluorescein–phosphonium)	GHB	Hydrogen-bonding-driven fluorescence enhancement	Ethanol–water suspensions	76.84 mM	Solvent dependence; limited green applicability	52
Biocompatible hybrid nanomaterial (DASH@SiO_2)	GHB, GBL, GVL	ICT-driven emission shift; vapor and solution sensing	Solution; vapor phase; solid	0.002 μM (GBL); 6.45 μM (GVL)	Early-stage platform; device integration needed	53
Lanthanide metal complex (Eu^{3+} sensitization)	Bromazepam	Antenna effect: coordination of bromazepam to Eu^{3+} enables ligand-to-metal energy transfer, producing characteristic Eu^{3+} emission	Ethanol solutions; pharmaceutical tablets; spiked serum	3 nM	Requires Eu^{3+} salts; solvent dependence (better in aprotic media); mainly applicable to bromazepam only	54
Lanthanide metal–organic framework (Eu-MOF)	Flunitrazepam	Photoinduced electron transfer (PET) and inner filter effect (IFE) causing Eu^{3+} emission quenching	Methanol–water suspension; urine; beverages; agarose gel	73 nM	Turn-off sensing susceptible to background quenching; methanol-dependent; high-temperature solvothermal synthesis	55
Carbon nanodots (N-doped CDs)	Clonazepam	Fluorescence quenching *via* interaction with nitro group, altering energy migration pathways	PBS buffer; human plasma; pharmaceutical tablets	12 nM	Requires instrumental fluorescence readout; not suitable for naked-eye detection	56
Hydrophobic carbon nanodots	Nimetazepam; other nitro-benzodiazepines	Photoinduced electron transfer without ground-state complex	Organic solvent systems (toluene, ethyl	7.24 μM	Requires non-aqueous media; limited direct applicability to beverages or	57

Table 1 *(continued)*

System	Analyte	Sensing mechanism	Sensing medium	LOD	Limitation	Ref.
		formation	acetate/dichloromethane)		biological fluids	
Ratiometric polydopamine nanoprobe (RhB-doped)	Clonazepam	Ratiometric fluorescence enhancement by suppression of π–π* energy loss; RhB as internal reference	Tris–HCl buffer; patient plasma	15.87 nM	Requires acidic conditions (pH 2.5); acetonitrile pretreatment for proteins; limited long-term stability	58
Quantum dots (Mn-doped ZnS) with molecularly imprinted polymer (MIP)	Diazepam	Molecular imprinting-assisted selective fluorescence quenching	Pharmaceutical tablets; human serum	87.8 nM	Template-specific recognition limits broader benzodiazepine applicability; synthesis complexity	59
Organic small-molecule solid-state fluorophore (carbazole–fluorene conjugate)	Ketamine	Aggregation disruption and hydrogen-bonding-induced conformational change leading to fluorescence enhancement in thin films	Solid thin film (paper); aqueous ketamine contact	0.04 μM (≈50 pg cm^{-2} on film)	Operates only in solid-phase contact mode; limited quantitative precision; requires UV excitation	60
Supramolecular host–guest AIE system (cucurbit[8]uril–palmatine complex)	Ketamine	Guest displacement from $(palmatine)_2$@CB[8] causing fluorescence quenching	PBS buffer; spiked urine samples	21 nM	Turn-off response; relies on supramolecular equilibrium; requires controlled buffer conditions	61
BODIPY–phenanthroline metal–organic probe with Cu^{2+}/Cu^{+} redox chemistry	Ketamine, scopolamine	Reduction of Cu^{2+} to Cu^{+} by ketamine followed by Cu^{+} coordination, inducing fluorescence quenching and color change	Aqueous/ethanolic media; drink matrices	2.88 μM	Micromolar sensitivity; temperature-dependent response; limited biological applicability	62
DNA-stabilized silver nanocluster (DNA–AgNC)	Ketamine	Ketamine binding to DNA recognition region induces structural rearrangement and fluorescence quenching	PBS buffer; forensic blood samples	0.25 nM	Poor photostability; DNA fragility; cold-storage dependence	63
DNA-capped gold nanoparticle–fluorescein system (FRET-based)	Ketamine	Ketamine-induced DNA reorganization inhibits FRET, leading to fluorescence turn-on; ATP-enabled regeneration	Aqueous buffer; laboratory samples	12 nM	Long incubation time (~90 min); complex probe architecture	64
Carbon dot–AuNP dual-mode nanocomposite	Ketamine	Ketamine binding to AuNP disrupts FRET and induces nanoparticle aggregation, giving fluorescence turn-on and color change	Non-alcoholic beverages	13 μM	Moderate sensitivity; relies on nanoparticle aggregation	65
Paper-based microfluidic trimodal sensor (CD–AuNP + PAN + $Co(SCN)_2$)	Ketamine	Combined fluorogenic (FRET disruption), chromogenic (Morri's test), and potentiometric responses	Paper-based device; aqueous ketamine solutions	3.2 μM	Multi-component fabrication; semi-quantitative readout	66

GHB) and 1,4-butanediol are reported for clandestine use. Although GHB is the most common of them all, due to more stringent drug management, it became hard to procure, and the less regulated prodrug GBL as well as GVL appeared as preferable replacement. GBL easily metabolises into GHB in the presence of lactonase enzyme in the body, and due to the lipophilic nature, it can be absorbed in higher quantities after oral ingestion.

A wide range of colorimetric sensors have already been commercialised, such as "Drinksafe™" cards and coasters, "Drink Detective™", "Safety straw" in 2011, and more recently colour changing nail polish "Undercover colour" which allowed the on-site detection of illicit date rape drugs.[37] The scope of these sensors was generally limited to analytes such as GHB, ketamine, or Rohypnol, and none of them provided a reliable method for detecting GBL, a key precursor of GHB. Therefore, a new, sensitive, and selective sensor for GBL that could operate under real beverage conditions was long due.

The first luminescent sensor for GBL was reported by Chang and coworkers in 2013. The research group from the National University of Singapore applied a diversity-oriented fluorescence library approach (DOFLA) to screen around 5120 new moieties and directed their attention to the most promising candidate sensor **5**, which was a BODIPY dye with two appended hydroxyl functional groups.[38] The sensor **5** was named as "**Green Date**". It furnished very sharp absorbance and emission maxima with small Stokes shift at 569 and 582 nm, respectively, which is a common characteristic of the BODIPY dye. To analyse the GBL sensitivity, a fixed stock of the **Green Date** was subjected to incremental addition of GBL from 0 to 100 mg mL^{-1} in water leading to a steady fluorescence enhancement up to 16 times of the initial emission (Fig. 3b). Furthermore, the same result was obtained when the GBL titration was executed either under varying pH of 2 to 11 or with high ethanol concentration (10%) (Fig. 3). The probe functioned over a wide pH range (2–11) and tolerated up to 10% ethanol, making it applicable to both alcoholic and non-alcoholic drinks. A substantial low limit of detection of 34.88 mM for GBL found in a 10% ethanol water mixture of sensor **5** required a thorough understanding of the sensor–analyte interaction.

The mechanistic investigation established that due to the hydrophobic nature, the Green Date molecules preferred to form nano aggregates in water, where the molecular emission was quenched from conventional static quenching after excimer formation. Upon GBL addition, the aggregates were disassembled and the increased radiative decay culminated

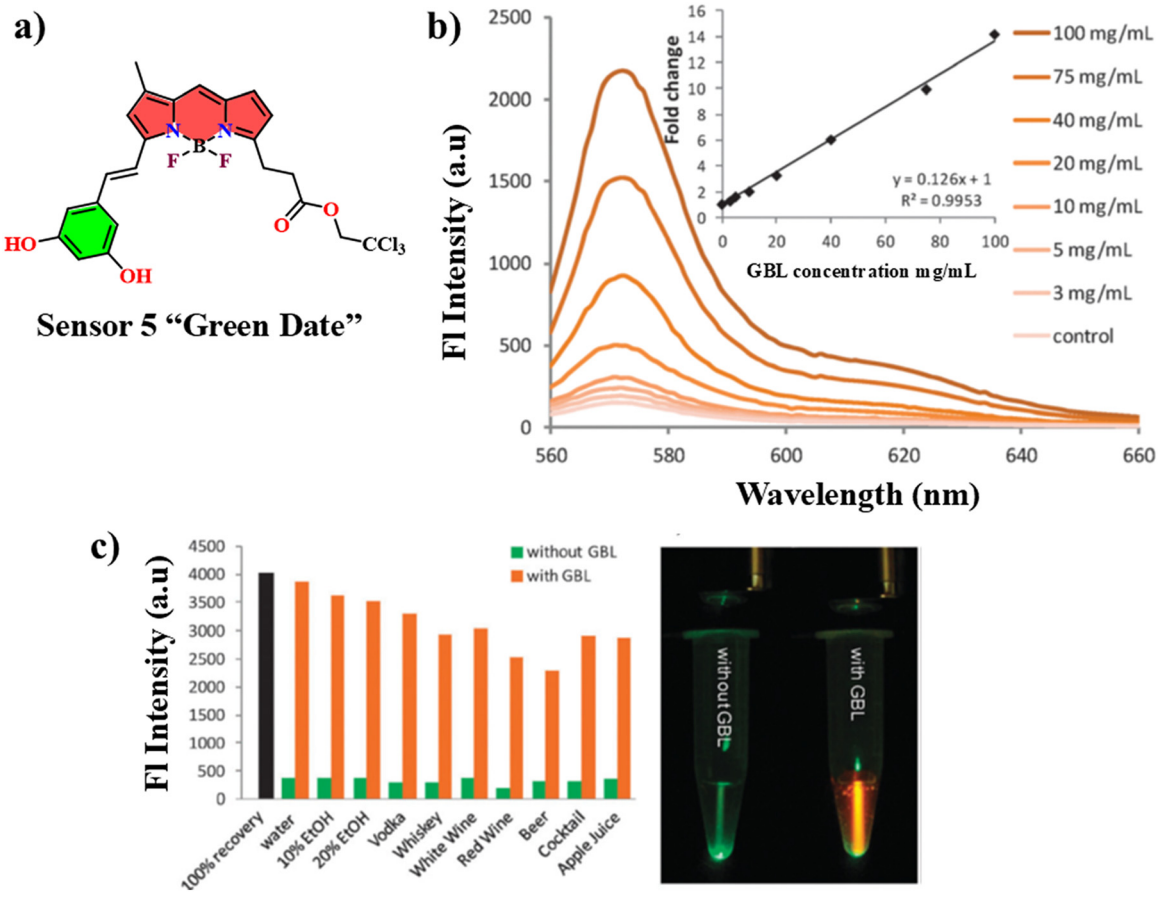

Fig. 3 (a) Structure of the fluorescent sensor **5**, (b) fluorescence titration of the sensor with GBL, and (c) selectivity of sensor **5** towards GBL. Reprinted with permission from ref. 38. Copyright 2013, the Royal Society of Chemistry.

into emission enhancement. The GBL-induced disassembly was further established using ^{19}F NMR, where the GBL addition led to the appearance of a strong single peak, originating from the BODIPY unit. Although Green Date furnished excellent GBL sensitivity, the performance waned under higher alcohol concentration, which limited the scope of practical applications.

Since Green Date was limited by alcohol interference and lack of selectivity, the same group modified the BODIPY framework and developed a GHB sensor **6**, which performed fluorescence detection at a very high alcohol concentration of 50% in water.[39] When compared with **Green Date** the new sensor termed "**GHB Orange**" furnished a minor hypsochromic shift in the absorbance and emission of 557 and 574 nm, respectively. On the contrary, incremental addition of GHB (0 to 100 mg mL^{-1}) to the sensor solution led to an 8-fold emission quenching (Fig. 4).

When the quenching behaviour was carried out in different solvents, in a 50% DMSO aqueous solution, maximum 5.5-fold reduction was induced with the addition of ~96.05 mM GBL. For practical application, various alcoholic beverages were spiked with GHB and subsequently exposed to **GHB Orange** solutions. Within 30 seconds of exposure, the emission intensity of drinks spiked with 5 mg mL^{-1} GHB reduced by 1.3-fold, whereas the controlled drinks remained unaffected. The result indicated the high sensitivity of sensor **6** in the detection of trace amounts of GHB in alcoholic drinks. A more detailed exploration was carried out to enquire the fluorescence quenching pathway and with the assistance of ^{1}H NMR titration experiment, it was established that GHB forms a stable hydrogen-bonded complex with the sensor and a steady photoinduced electron transfer from the GHB core to the probe caused fluorescence quenching. The sensor established a highly sensitive platform for the development of a commercial sensor, but in reality, the interference from other drugs as well as carboxylic acids jeopardised the sensor response.

The GHB class of drugs are mostly used in DFSA but often times a combination of other drugs such as LSD and synthetic cathinones (SCs) are used to synergistically enhance the effect of GHB, and hence, the detection of their presence is crucial. In this regard, Nuevalos and coworkers have modified the previously mentioned BODIPY core and decorated the periphery with hydrazone and benzothiazole units to afford sensor **7** and **8**, respectively.[40] After extensive characterisation with different spectroscopic and spectrometric techniques, the systems were subjected to photophysical analysis. For sensor **7**, a major absorption peak at 584 nm was associated with a minor peak at 717 nm, whereas the exited sample furnished bright emissions at 616 nm in DMSO. Sensor **8** also furnished comparable photophysical traits with a slightly higher quantum yield of 0.95.

When subjected to the addition of Na-GHB to the sensor, the main absorption peak at 584 of sensor **7** was diminished with a concomitant enhancement of the 717 nm peak (Fig. 5a). Moreover, the emission intensity drastically reduced. The photophysical changes of sensor **7** and **8** was found to be influenced by the very lowest concentration of 0.4 μM and 0.3 μM of Na-GHB as obtained from the titration experiments, which is well below concentrations found in spiked beverages.

Interference tests with citric acid, sucrose, and ascorbate confirmed reliable performance, and the probes were validated in soft drinks, producing immediate visual changes under a UV lamp. Furthermore, to evaluate the cathinone sensitivity, the sensors were transformed into their Cu(II) complexes, and subsequently, their photophysical responses were monitored. Cathinones such as ephedrone, 3,4-methylenedioxy-α-pyrrolidinohexiophenone (MDPHP), 4′-methyl-α-pyrrolidinohexiophenone (MPHP), and 3,4-methylenedioxy-*N*-methylcathinone (MDMC) reduced Cu(II) to Cu(I), triggering fluorescence quenching with a detection limit of 2.0 μM.

Although GHB sensors were developed employing sensitive fluorescence changes, same research went one step further by using a combinatorial approach of developing GHB sensors with both fluorogenic and chromogenic

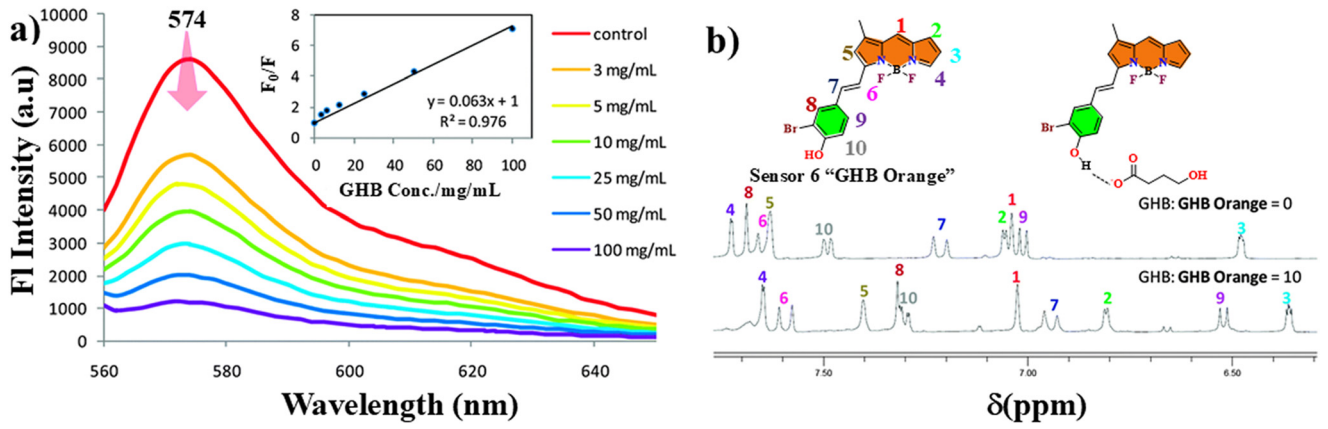

Fig. 4 (a) Fluorescence titration of sensor **6** with GHB, and (b) change in the ^{1}H NMR spectra of **6**, before and after the addition of GHB. Reprinted with permission from ref. 39. Copyright 2014, the Royal Society of Chemistry.

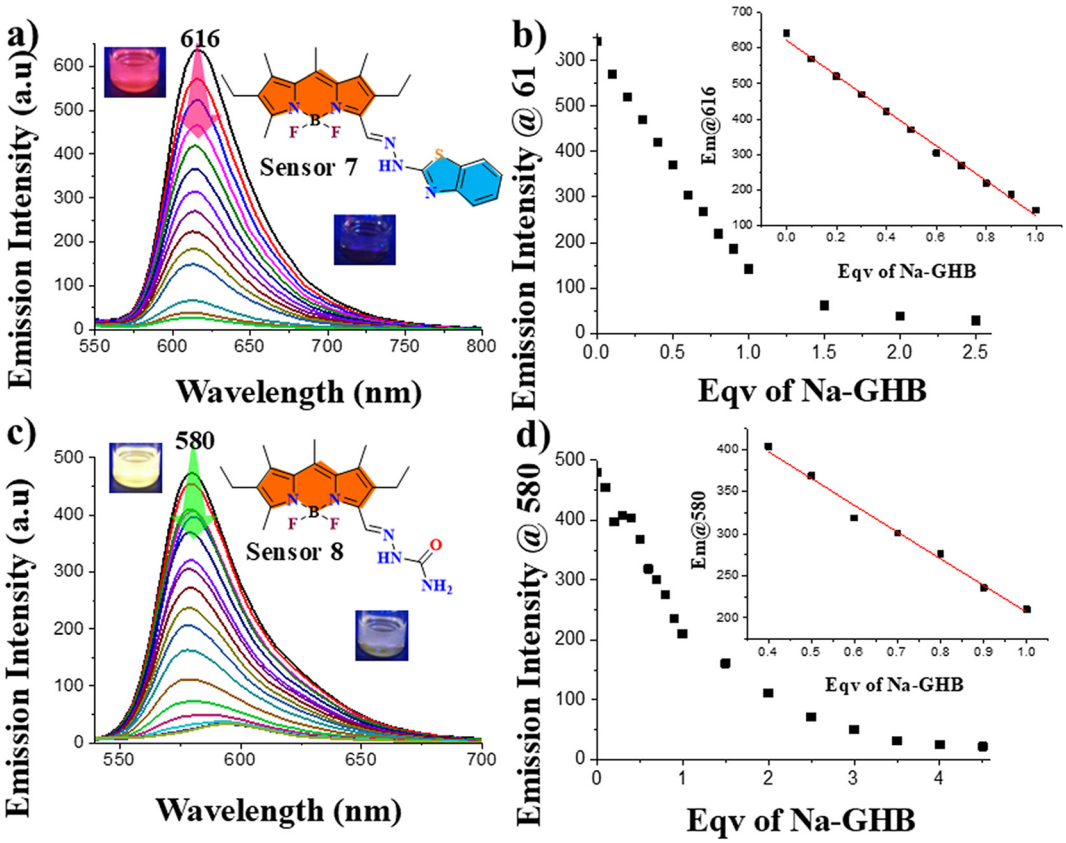

Fig. 5 a) Observed fluorescence changes of sensor **7** (5 μM in DMSO, λ_{ex} = 500 nm) with increasing quantities of Na-GHB (0–2.5 equiv.). b) Changes in fluorescence at 616 nm of **7** upon the addition of increasing amounts of Na-GHB and its linear regression. c) Emission spectra changes observed for sensor **8** (5 μM in DMSO, λ_{ex} = 450 nm) with increasing quantities of Na-GHB (0–4.5 equiv.). d) Emission changes at 580 nm of **8** upon the addition of increasing amounts of Na-GHB and its linear regression. Reprinted with permission from ref. 40. Copyright 2022, Elsevier B.V.

responses. Two new napthoxazole derivatives **9** and **10** were designed, synthesized, and thoroughly characterised. Probe **9** contained an electron-deficient nitro group, whereas **10** was decorated with a fluorescein moiety. Both probes **9** and **10** displayed broad absorption bands at 355 and 370 nm, respectively.[41]

Their emission profile analysis revealed that sensor **9** was non-emissive due to the presence of an electron-deficient nitro group and **10** produced weak fluorescence at around 541 nm, originating from the fluorescein unit. When the DMSO solutions of the compounds were exposed to incremental GHB doses, the absorbance spectra of both **9** and **10** ratiometrically shifted to new peaks at 500 and 490 nm, respectively. The change in absorbance was also associated with the observable visual changes in red and yellow colouration of the solutions. More crucially, the visible colour change of **10** was also accompanied by a strong emission enhancement, and the associated titration profile provided a very low detection limit of 0.12 μM or GHB (Fig. 6). When ^{1}H NMR titration was utilised to examine the sensor–analyte interaction, an up-field shift of all aromatic protons was observed, indicating that GHB-induced deprotonation was responsible for the emission enhancement. Furthermore, the sensitivity of the compounds towards GHB was tested by spiking the drug into different alcoholic beverages, where superior performance by sensor **10** due to its bright turn-on fluorescence highlighted the potential for nightclub environments.

The solution-phase detection of GHB class of drugs have been elaborately explored by developing a wide array of organic small molecule-based sensors, but the analysis method suffers from some critical drawbacks such as requirement of a proper organic solvent medium for better emission and a smartphone to analyse the readout and poor detection limit under aqueous conditions. As a suitable alternative, Gavina and coworkers developed a paper strip-based luminescent sensor based on 2-amino napthtoxazole and benzoxazole building blocks.[42] The core structure was decorated with fluorescein to afford sensors **11** and **12**, and its methylated analogue **13** (Fig. 7a). The formation of the target molecules was extensively investigated using multinuclear spectroscopy and mass spectrometry analyses. During the investigation of the solid-phase optoelectronic behaviour, sensor **12** furnished broad absorption peaks at 300 nm along with a 370 nm shoulder giving rise to the yellow coloration of the sensors. When the sample solution of **12** was exposed to GHB, the emission intensity at 532 nm steadily increased with the increase in analyte concentration,

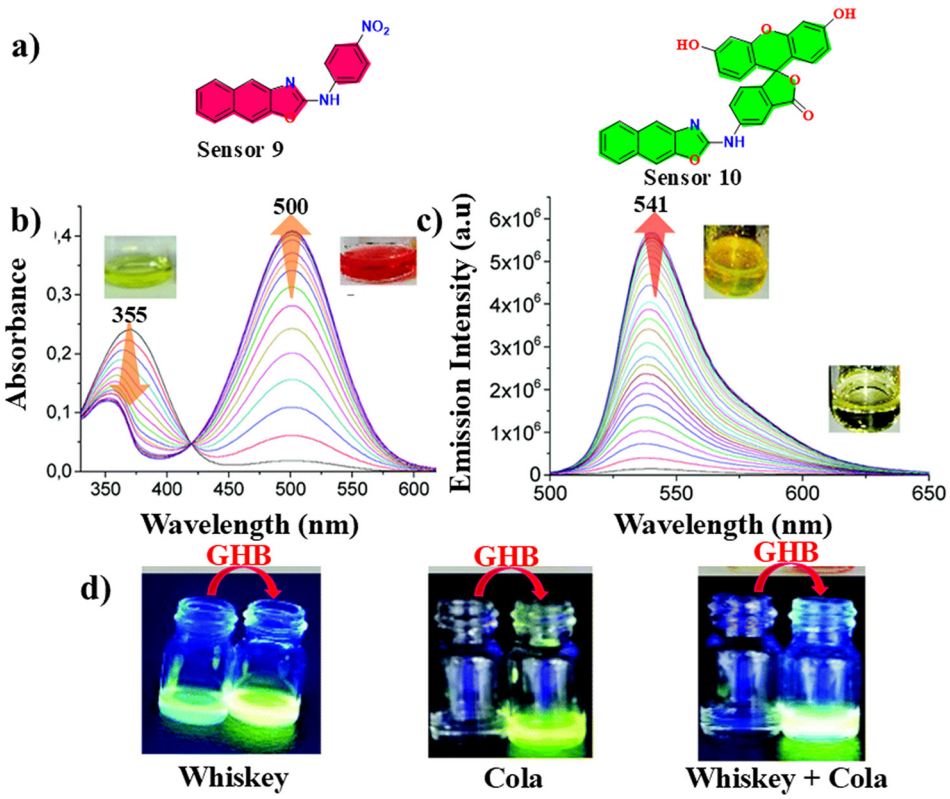

Fig. 6 a) Structures of sensors **9** and **10**; change in the absorbance of sensor **9** (b) and emission of sensor **10** (c) after titrating with GHB, and d) images of sensor **10** under UV light in the presence of GHB-spiked drinks of whiskey, cola and a mixture of both (left to right). Reprinted with permission from ref. 41. Copyright 2020, the Royal Society of Chemistry.

and using the titration curve, the limit of detection was estimated to be 0.06 μM. Similar photophysical responses were obtained during the photophysical analysis of **13**.

For practical applications, fluorescent paper strip-based sensors were prepared by saturating cellulose paper disks with a sensor solution followed by drying at room temperature. When a low concentration of GHB was spotted on the cellulose paper, a bright fluorescent spot gradually developed with time, indicating efficient GHB sensing properties of the paper strip. For sensor **11** on the contrary, the addition of GHB was associated with a ratiometric signalling with a steadily increasing peak at 528 nm along with a gradual depletion of the major emission peak at 405. The limit of detection was estimated to be 0.45 μM. Selectivity tests against GBL, scopolamine, diazepam, ketamine, and ephedrine showed no false positives under the reported conditions. Another strength is the low cost, portability, and use of green chemistry principles, since no organic solvents are needed and cellulose is biodegradable. The system thus represents a sustainable and user-friendly platform that could realistically be deployed in pubs, clubs, and similar social gatherings for rapid screening. The main limitation, however, is that its sensitivity remains in the millimolar range, which is sufficient for detecting spiked drinks but not suitable for forensic or clinical analysis of biological fluids.

Emphasizing the need for more sensitive and cheaper paper-based sensors, Xincun Dou and others developed a series of 2-(2′-hydroxyphenyl)benzothiazole (HBT)-based sensors **14**–**17**.[43]

The polar nature of GHB and its hydrogen bonding affinity towards nitro groups were further extrapolated by the authors who decorated electron-rich benzothiazole with both electron-donating and -withdrawing amino and nitro groups, respectively. The selection for such functionalisation was that GHB will exhibit different types of weak interactions with numerous functional groups, which would induce changes in their photophysical properties. The compounds **14** and **15** were found to be unresponsive towards GHB, but the unsubstituted **17** furnished a marked emission enhancement at 472 nm (Fig. 8a). When an electron-withdrawing nitro group was introduced, a marked emission quenching was observed for sensor **16**.

The authors proposed that the sensor **16** weakly interacted with GHB *via* hydrogen bonding, leading to the loss of radiative energy, whereas the sensor **17** underwent a keto–enol tautomerism and the mission drastically enhanced. Instrumental LODs calculated from calibration were 660.87 nM for the colorimetric mode and an outstanding 5.62 nM for the fluorescent mode for the sensors **17** and **16**, respectively.

All the aforementioned organic small-molecule sensors were developed based on the emission of individual sensors,

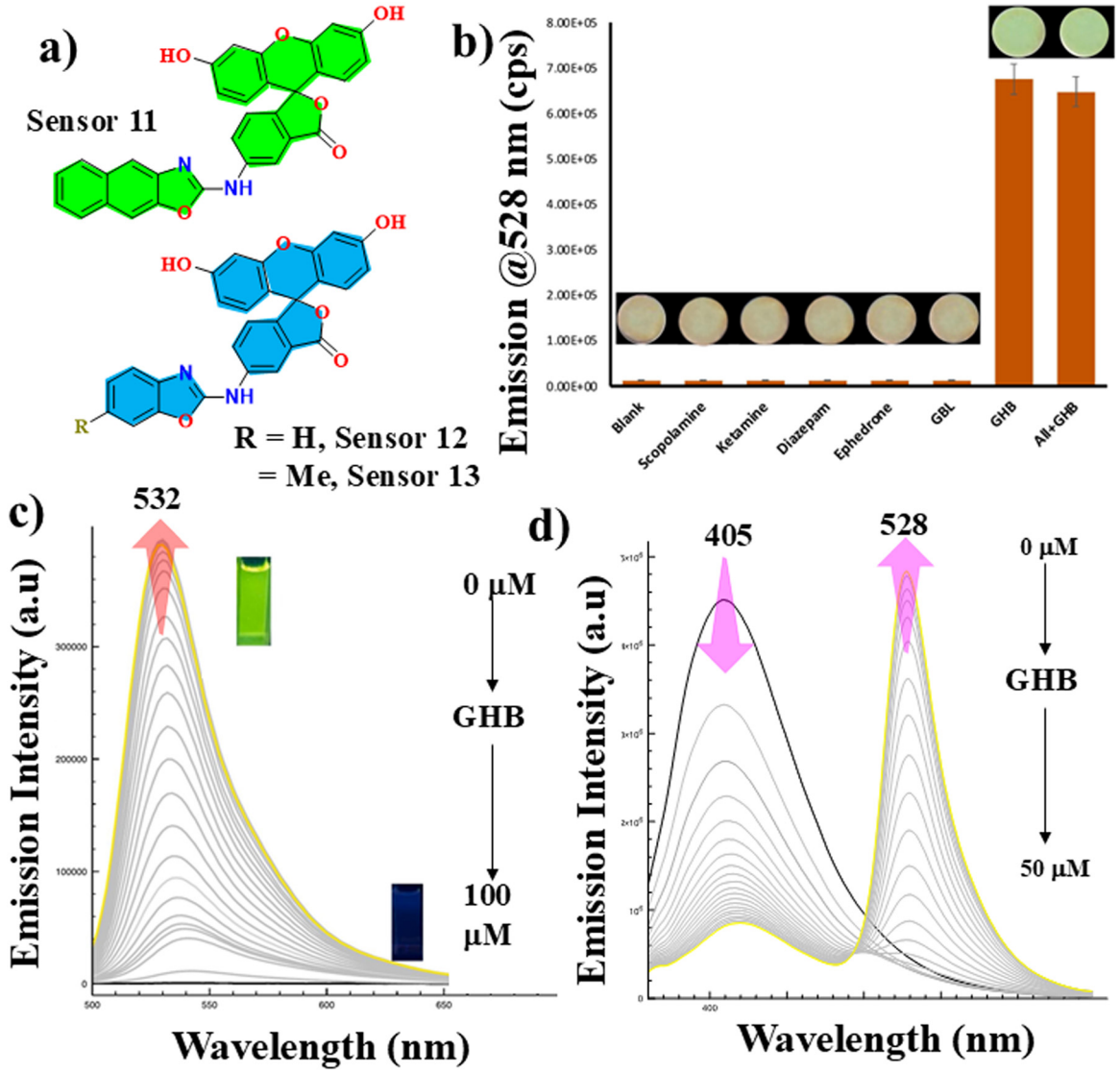

Fig. 7 (a) Structure of sensors **11**, **12**, and **13**; (b) solid-state response of sensor **11** upon exposure to different narcotics; emission profiles of sensor **12** (c) and sensor **11** (d) with the incremental addition of GHB. Reprinted with permission from ref. 42. Copyright 2024, Elsevier B.V.

but Kanvah *et al.* went forward with the first report of a new type of fluorene-based cyanostillbene sensor with unique aggregation-induced emission behaviour. A series of analogues fluorescent probes **18**–**21** were developed with changing peripheral functional groups.[44]

During photophysical experiments, dioxane solutions of all the sensors displayed a strong AIE behaviour with high water fractions. When water was added incrementally to the dioxane solution of sensor **21**, the intensity of the main absorption peak at 362 gradually decreased and the shape of the peak got broadened along with the appearance of a long wavelength tail. Such spectral broadening and long tails are often associated with the Mie scattering from suspended aggregates in the medium.[45–47] The SEM analysis revealed a wide range of aggregate morphologies including oval (**18**), spherical (**20**), and wire (**21**) with sizes ranging from 130 to 250 nm (Fig. 9c). Moreover, when the sensors were exposed to GHB only the hydroxyl group appended fluorophore **21** furnished noticeable fluorescence changes. As observed previously, the hydroxy functional group of **21** formed a strong hydrogen bond with GHB, which resulted in an optoelectronic change. The key emission peak of sensor **21** at 434 nm steadily decreased with the rapid emergence of a new peak at 550 nm, giving rise to a favourable ratiometric response, accompanied by a visible blue-to-yellow colour change.

The authors made simple paper strips coated with compound **21** that furnish visual colour changes with a low GHB concentration of 5 mM GHB (with a stronger, obvious colour at ~20 mM), making the strips suitable for on-site beverage screening. Other derivatives behaved differently. When the water fraction was substantially high in the experiments, compound **20** (NO_2) showed the maximum AIE with 120-fold emission enhancement. The key limitations of

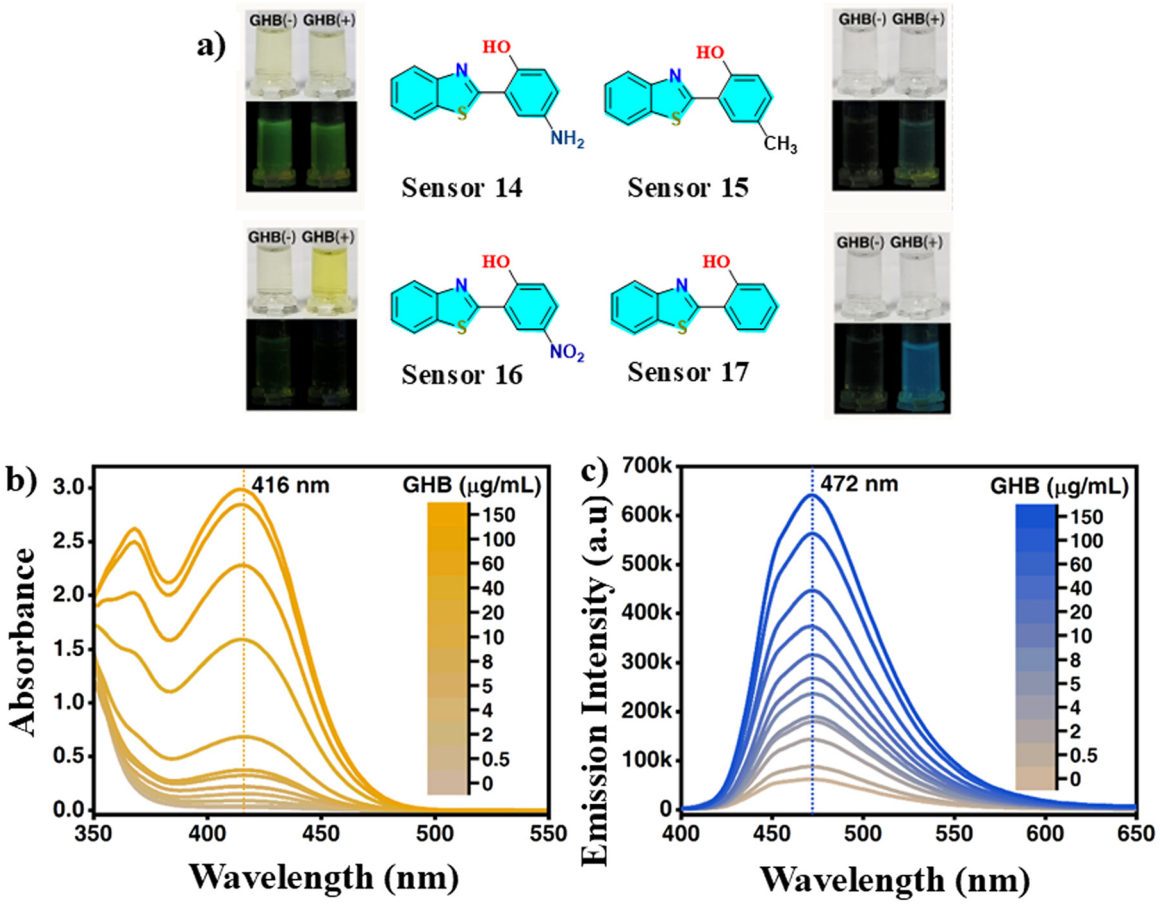

Fig. 8 (a) Changes in the emission along with the structures of the sensors **14**–**17** before and after GHB addition. Influence of GHB addition on the absorption (b) and emission (c) profiles of **17**. Reprinted with permission from ref. 43. Copyright 2024, the American Chemical Society.

the probes are the relatively high analyte detection concentrations (millimolar range), emission perturbation based on changing alcohol fraction, and limited validation in real biological fluids. Thus, the probes were practical for quick on-site drink checks but not suitable for trace detection in blood or urine.

3.2. Luminescent sensors based on metal complexes

The small organic building blocks were designed to afford sensitive and selective sensors for the GHB class of drugs, where different fluorescence responses including quenching, enhancement, and ratiometric switching were furnished. However, such responses often suffer from strong background emissions, poor sensor lifetime, low emission quantum yield, *etc.* Paper-strip adaptations improved portability but often sacrificed sensitivity, with detection limits in the millimolar range, far above the concentrations relevant to forensic analysis. In this regard, the transition metal complex-based luminescent systems appeared to be a preferable alternative to the conventional sensors due to several additional advantages such as i) long emission lifetime from the mixed metal–ligand states, ii) minimised self-quenching due to well-separated absorption and emission, and iii) substantially high luminescence quantum yields. Considering these advantages, the research group of D.-L. Ma has developed the first GHB sensor **22** based on a transition metal complex platform.[48] The sensor consisted of an iridium core and was surrounded by bipyridine and phenanthroline ligands (Fig. 10a). With 300 nm excitation, a strong emission at 570 nm with a long lifetime of 4.83 μS was observed. The very large 270 nm Stokes shift was substantially high compared to the aforementioned organic probes, which eliminated the issue with self-quenching. To evaluate the analyte sensitivity, an aqueous GHB solution was added gradually to luminophore **22** in water and within 10 s, a steady quenching of the emission occurred. The maximum 60% quenching was induced when the GHB concentration was 12.4 mM. The sensing mechanism involved GHB binding-induced perturbation of the excited-state configuration of the complex, which suppressed the phosphorescence.

For a practical scenario, numerous drinks such as red wine, whiskey, and orange juice were spiked with GHB and exposed to a low concentration of the senor of 1.44 mM, which culminated into discernible emission quenching. Most importantly, the long lifetime enabled the analyte analysis *via* time-resolved emission spectroscopy (TRES), which

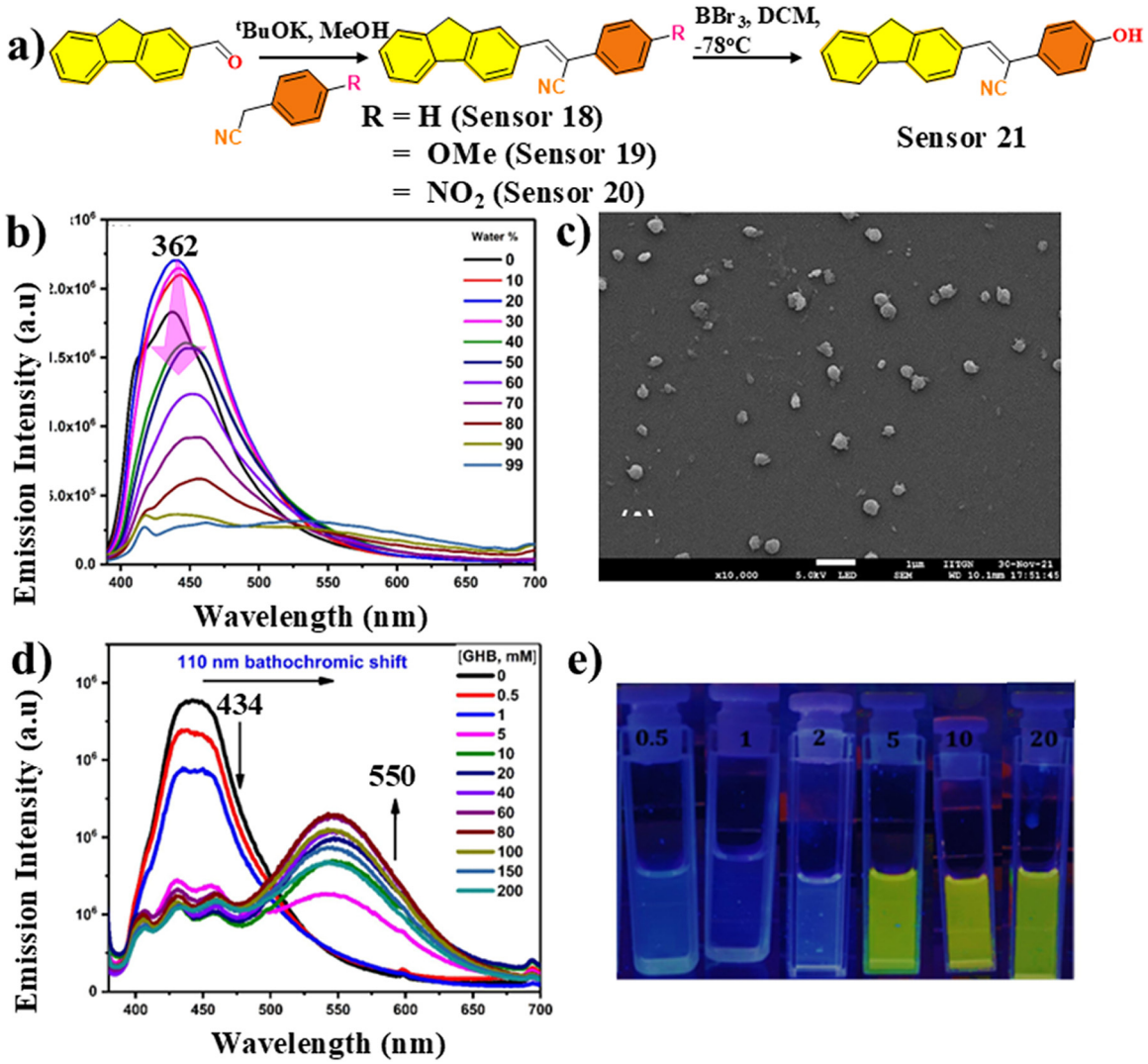

Fig. 9 (a) Structures of sensors **18**–**21**, (b) change in the absorption spectra of **21** with increasing water fraction in dioxane, (c) SEM image of the aggregates, (d) ratiometric emission response of **21** with increasing GHB fraction, and (e) images of the vials of solution of **21** with different GHB concentrations. Reprinted with permission from ref. 44. Copyright 2022, Elsevier B.V.

filtered out background autofluorescence from coloured drinks, significantly enhancing the signal-to-noise ratio.

The Ir(II) complex furnished strong GHB selectivity and sensitivity, but for low-cost commercial sensors, more affordable first-row transition metal complexes would provide better opportunity. A new BODIPY–Fe(III) metal complex **24** was developed by Kim and Ryu, which mitigated the concern for the expensive sensors.[49] This indicator-displacement design produced a rapid "turn-on" response, with bright fluorescence and visible colour recovery within five seconds. The design of the metal complex was such that the molecule retained sensing capabilities under altered polarity, over a long pH range and even in the presence of different interferences. The addition of a Fe(III) salt solution to the free ligand **23** led to a diminished absorbance at 502 nm and the appearance of a new peak at 520 nm. Following the same trend, a new emission peak emerged at 588 nm at the expense of the ligand emission at 555 nm. The authors proposed that the addition of the GHB lead to dismantling of the metal ligand bond owing to the affinity of more labile and electron-enriched carboxyl group of the GHB compared to the ligand –COOH towards the Fe(III) centre.

When GHB was added to the Fe(III)–BODIPY complex, the original absorbance at 520 nm changed immediately to 505 nm and the change was attributed to free ligand generated after disintegration of the metal complex. The change in the absorbance induced a ratiometric response in the emission of the sensor (Fig. 11b). Absorption and fluorescence titration with GHB indicated that a meagre 2 mg mL^{-1} GHB was enough to induce a 17-fold emission enhancement, and the limit of detection was found to be 2.40 μM. When the fluorescence sensitivity of the Fe(III)–BODIPY complex was monitored using interferences such as fentanyl, lorazepam, and alprazolam, no discernible changes occurred, indicating the superior selectivity of the sensor. To make the sensor practical, the team fabricated cellulose acetate strips impregnated with the Fe^{3+} complex, which enabled portable, on-site detection using a simple

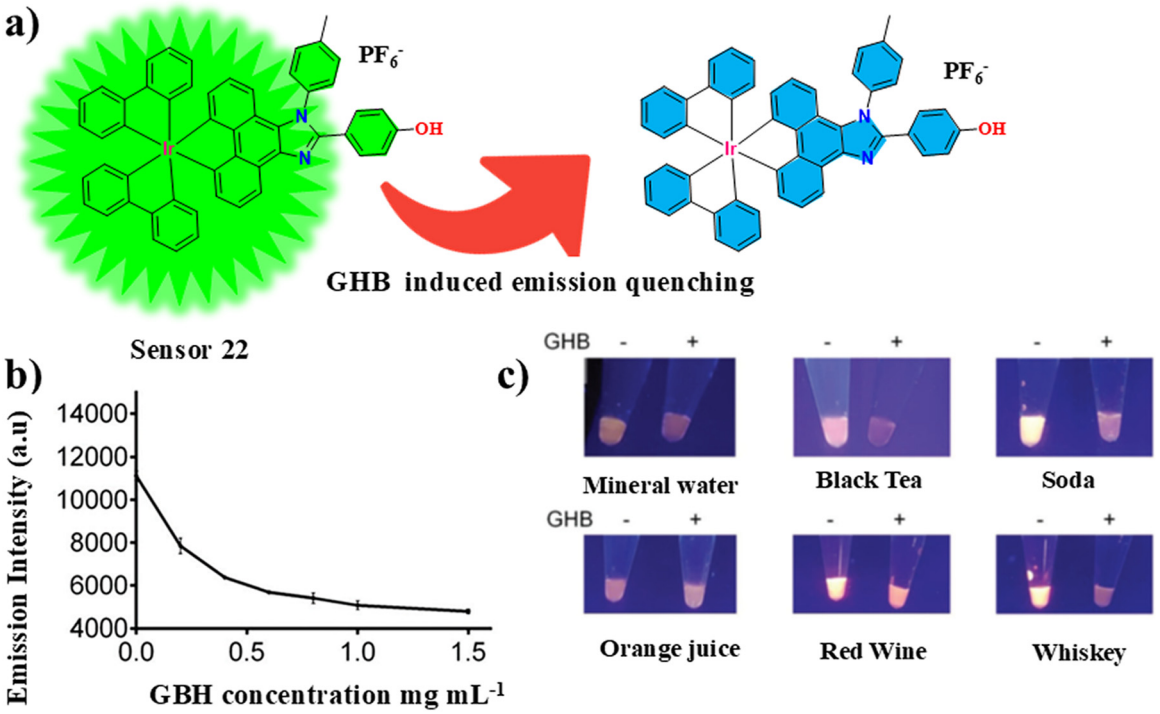

Fig. 10 (a) Schematic of the sensing of complex **22**, (b) luminescence titration with the varying GHB concentrations, and (c) change in the emissions of different spiked beverages under UV light. Reprinted with permission from ref. 48. Copyright 2013, the Royal Society of Chemistry.

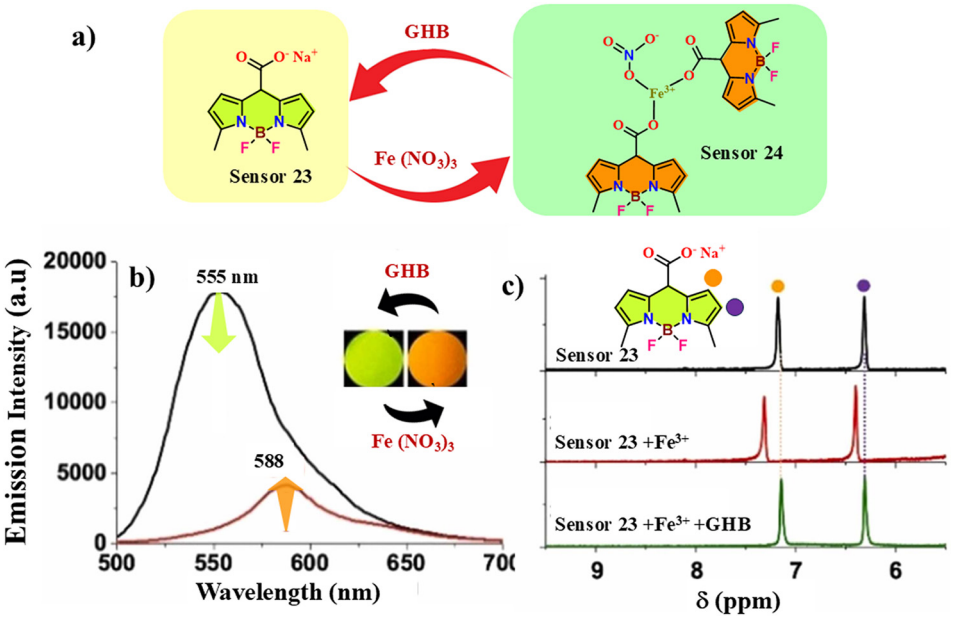

Fig. 11 (a) Complexation-induced structural and photophysical changes of sensors **23** and **24**, (b) change in emission peaks with the addition of an Fe(III) salt to sensor **23** and (c) corresponding ^{1}H NMR spectra. Reprinted with permission from ref. 49. Copyright 2022, Elsevier B.V.

smartphone readout. Despite its excellent speed and sensitivity, this system required careful strip preparation for reproducibility, and some complex beverages still needed dilution to reduce interference. Moreover, the presence of metal salts raised concerns about strip stability and shelf life.

Taking que from this concept of ligand displacement-based fluorescence switching, Manez *et al.* developed an even more simple coumarin–Cu(II) complex **25** for GHB detection.[50] The triflate salt of the Cu(II) quinoline complex was treated with coumarin carboxylic acid to afford the targeted sensor **25** (Fig. 12a). The formation of the sensor was analysed using multinuclear NMR and other spectroscopic methods, and was equivocally established with mass spectrometry analysis. Using the ligand displacement

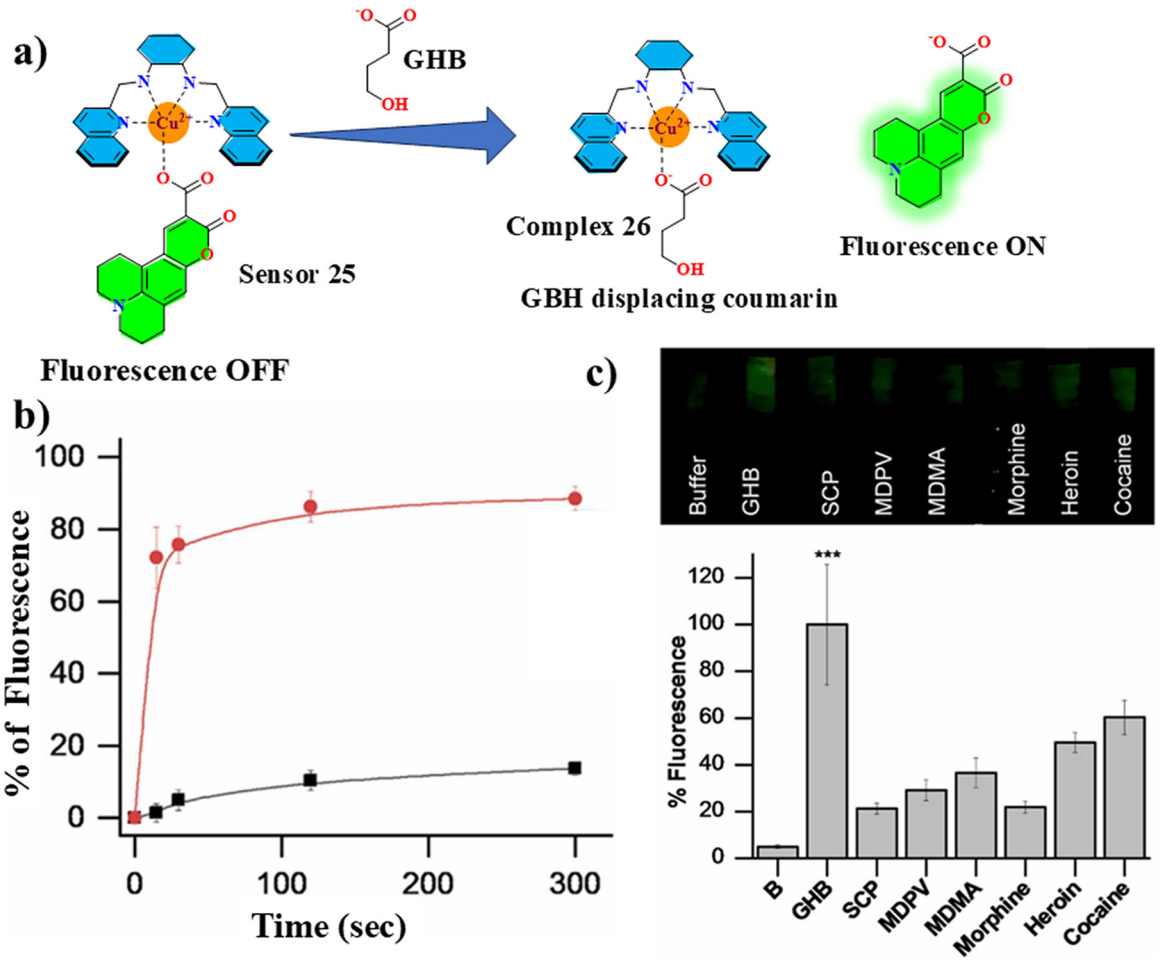

Fig. 12 (a) GHB-induced structural changes on sensor **25**, (b) effect of time on the fluorescence of sensor **25**, and (c) selectivity of the sensor in the presence of interfering narcotics. Reprinted with permission from ref. 50. Copyright 2023, Elsevier B.V.

theory, it was proposed that the emission of the free coumarin ligand at 494 nm would be quenched upon complex formation with the paramagnetic metal centre. The GHB addition would lead to faster and more stable complexation with Cu(II) followed by a rapid coumarin displacement from the coumarin–Cu(II) complex, leading to the release of free coumarin in the system, which would be reflected in emission enhancement.

As predicted, the GHB addition led to a surge in the emission at 494 nm from the free coumarin, and the sensitivity was found to be as low as 0.06 μM. Apart from the strong sensitivity, when the interferences of other substances such as morphine, MDMA, heroin, and cocaine were investigated, the emission profile remained unchanged, also indicating the strong selectivity.

For practical applications, strips of the sensor were prepared where the strip consisted of a polyethylene glycol-coated glass fibre (PEG-GF) membrane, and the protocol used small sample volumes (≈75 μL). When applied to two-fold diluted beverages (*e.g.*, wine and gin), the strip detected GHB down to 0.1 μM after a 1 min dip and smartphone readout. Selectivity was tested against cocaine, heroin, MDPV, scopolamine, MDMA and morphine with negligible interferences with coefficients/error bars reported as 3σ for triplicates. This strip system offered clear advantages, as it delivered results in just one minute, achieved ultra-low detection limits (0.03 μM in buffer, 0.1 μM in beverages), and was easily read using a smartphone-based setup. Such portability made it suitable for on-site checks without specialized lab equipment.

3.3. Fluorescent nanomaterials for GHB sensing

Compared to the small organic molecules and individual metal complexes, the nanomaterials provide an additional advantage of signal amplification. The small-molecule sensor signal originates from a cumulative one-to-one interaction between each sensor and the analyte, thus the signal amplification is impossible, whereas, for nanomaterials owing to the higher surface area and the well-controlled band gap, the excited state energy can migrate through the architecture, leading to the quenching of all the sensors together. The higher quenching capability will reflect a lower response time of the sensor, thereby giving access to quick

detection and necessary medical treatment of the victim and apprehension of the culprit. Moreover, the nanomaterials are easy to prepare, fabricate and can seamlessly be moulded or incorporated into any solid platform to design solid or vapor-phase sensors.

Gavina *et al.* have demonstrated the chromogenic and fluorogenic GHB response from a pair of sensors **27** and **28** prepared by functionalizing silica nanoparticles with a napthoxazole platform and nitro and fluorescein functionalities, respectively.[51] The anchoring organic molecules were prepared, characterised and subsequently implanted onto commercially available LUDOX silica nanoparticles. The final sensors were examined using a DLS analyser and TEM to confirm the formation of functionalised nanoparticles, which provided average sizes of 16.2 ± 1.9 nm and 16.6 ± 2.0 nm for sensors **27** and **28**, respectively (Fig. 13c).

Suspended solutions of the sensors in a DMSO water mixture were exposed to different GHB concentrations, and the absorbance and emission were monitored for sensors **27** and **28**, respectively. A suspension of sensor **27** displayed a major and a minor absorption peak at 370 and 516 nm, respectively, and GHB exposure resulted in the gradual appearance of a peak at 516 nm in expense of the peak at 370 nm. On a similar note, the non-emissive suspension of sensor **28** turned into brightly fluorescent with emission enhancement at 534 nm after the GHB addition. The limit of detection was estimated using the titration of the analyte with the sensor and was found to be 96 mM and 1.65 mM for sensors **27** and **28**, respectively. For solid-state sensing, the nanoparticle was deposited on silylated cellulose papers and very low mM concentrations of GHB-induced optical responses on the paper sensors. Exposure to only 15 mM GHB resulted in discernible chromogenic and fluorogenic changes for sensor **27** and **28**, indicating strong potential for practical applications and commercialisation.

While the aforementioned nanomaterial-based sensors enabled solid-state usability and extension into saliva testing, they faced challenges with the reproducibility of fabrication and reduced sensitivity on immobilization. Some dependence

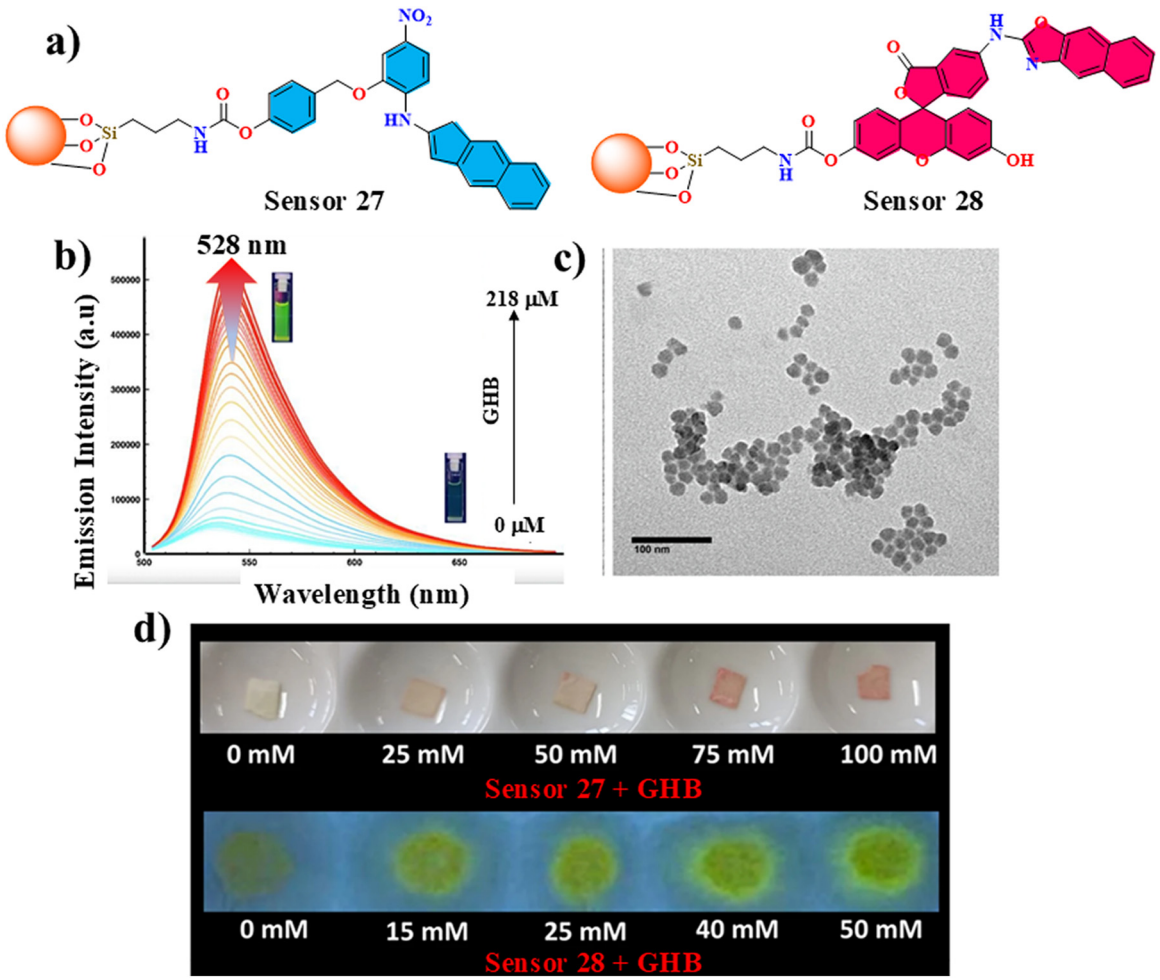

Fig. 13 (a) Silica-anchored nano sensors **27** and **28**, (b) fluorescence titration of sensor **28** with incremental addition of GHB in DMSO upon excitation at 490 nm, (c) TEM image of sensor **28**, and (d) chromogenic (top) and fluorogenic (bottom) responses of silylated paper saturated with sensors **27** and **28** with different concentrations of GHB under naked eye. Reprinted with permission from ref. 51. Copyright 1966, Springer Nature B.V.

on organic co-solvents also limited their "green" applicability. Consequently, the attention shifted to ionic liquid-based nanoparticles, which offered tuneable solubility, stable particle formation, and intrinsic fluorescent properties when coupled with dyes, making them a promising direction for future GHB sensors. Narcisse and coworkers have reported an ionic liquid **30** by combining trihexyltetradecylphoshonium cations along with fluorescein disodium salt **29**.[52] The ionic liquid was further transformed into nanoparticles by judicious employment of solvent composition, which led to enhanced surface activity and better sensitivity. The as-prepared ionic liquid and the nanoparticles were thoroughly characterised using a multinuclear NMR instrument, a DLS system, and a zeta potential analyser, which established an average particle size of 199 ± 76 nm with a polydispersity index of 0.1. The sensor **30** furnished strong absorption and emission at 515 and 536 nm, respectively, when dissolved in ethanol. When the ethanol stock was suspended in deionised water using a sonicator, nano particles were generated, and a minor bathochromic shift in the peak positions was observed for both absorption and emission.

When GHB was added to the nano particle suspension, steady enhancement was observed for both the UV and fluorescence peaks. Moreover, when the interferences from other recreational drugs such as butane diol and propionic acid were examined, the nanoparticle photophysical behaviour was found to be unaltered, indicating strong GHB affinity (Fig. 14c). The authors proposed a weak hydrogen bonding interaction between the ionic liquid and GHB, as the reason for the selectivity, and further mechanistic analysis was due.

Although all the aforementioned sensors were designed for the detection of date rape drugs, in none of the cases, the cell viability or toxicity analysis was carried out. For practical applications, it is utmost important to evaluate the effect of the sensor on humans, as the sensing mechanism involves contact between the sensor and suspected beverages. Keeping this in mind, Dhir *et al.* have recently developed a luminescent dansyl-carbazole (DASH) combination sensor **33** for the detection of illicit date rape drug as well as latent fingerprint.[53] Moreover, the gamma-valerolactone, a recreational drug with potency,

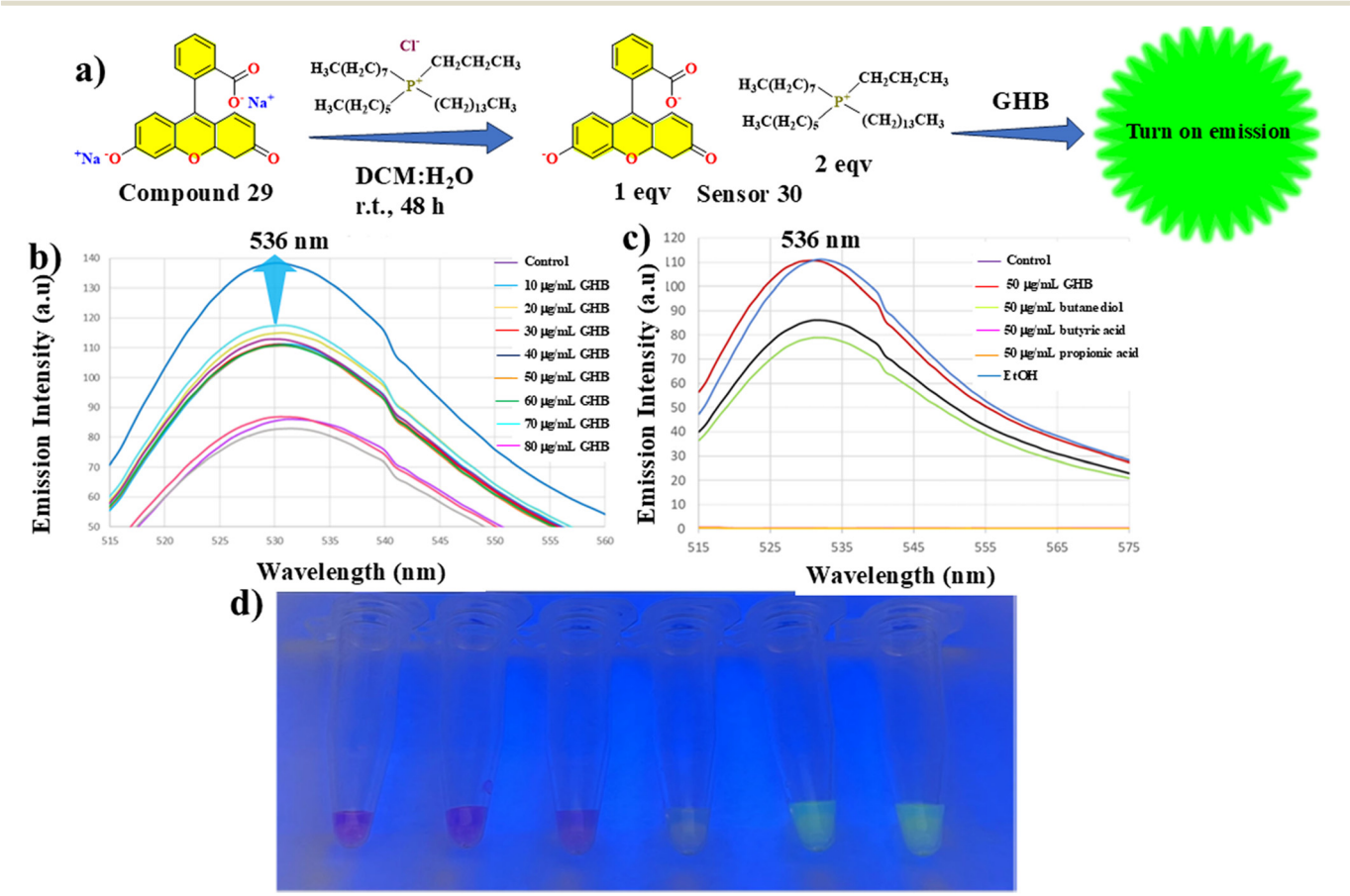

Fig. 14 (a) Synthetic scheme of sensor **30** from precursor **29** *via* ionic liquid formation, (b) gradual fluorescence enhancement with increasing GHB concentration, (c) effect of the interference of other common additives on the fluorogenic GHB response, and (d) change in the emission colour of sensor **30** under UV light after GHB addition. Reprinted with permission from ref. 52. Copyright 2025, authors and MDPI, Basel, Switzerland.

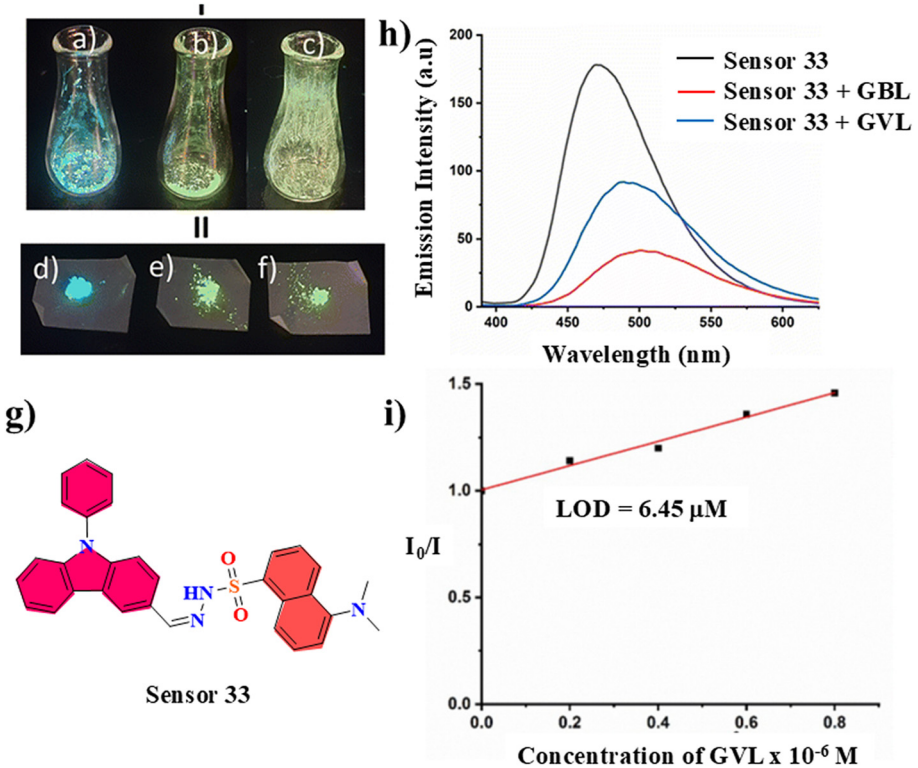

Fig. 15 Solid state response of the sensor **33** (a) after exposure to vapour of GBL (b) and GVL (c) as well as in drinks non-spiked (d) and spiked with GBL (e) and GVL (f). (g) Structure of the sensor **33** and (h) change in the emission of sensor solutions upon exposure to GBL and GVL. (i) Limit of detection for GVL estimated from fluorescence titration. Reprinted with permission from ref. 53. Copyright 2025, Royal Society of Chemistry.

similar to that of GHB was reported to influence detectable optoelectronic changes of the sensor **33**, leading to the first report for both GBL and GVL sensors. To elucidate the fingerprinting identification, the sensor was anchored on silica nanoparticles, leading to the sensor **33**@SiO_2 derivative. Sensor **33** was prepared by using an imine condensation reaction between carbazole aldehyde **31**, and dansyl hydrazine **32** in ethanol (Fig. 15g). The formation of the final compound was established by ^{1}H and ^{13}C NMR as well as high-resolution mass spectrometry. Photophysical characterisation displayed that when excited at 365 nm, a strong emission at around 470 nm appeared for DASH. The addition of GHB and GBL to the sensor solution led to a bathochromic shift, leading to yellowish emissions. Moreover, when the solid sensor was exposed to GBL and GVL vapors, a similar sensing capacity was exhibited. The limits of detection of the GBL and GVL fluorescence titration were evaluated to be 0.002 and 6.45 µM.

Finally, biological studies were carried out with NIH-3T3 cell lines by MTT-based cell viability assay, which established that when treated with a wide range of sensor concentrations (0–40 µg mL^{-1}), the cell viability was as high as 82%. The authors proposed that due to such high cell viability, the sensor can safely be used for on-field applications.

4. Fluorescent sensors for benzodiazepine class of illicit date rape drugs

Unlike the GHB class of date rape drugs, which mostly consist of only five available analytes, the benzodiazepines consist of a wide array of substrates with a similar structural backbone and comparable efficacy. The substrates and their common street names are flunitrazepam (Rohypnol), diazepam (Valium), chlorodiazepam (Librium), bromazepam, clonazepam (Klonopin), alprazolam (Xanax), lorazepam (Ativan), nimetazepam (Lavol), temazepam (Restoril), midazolam (Versed), clobazam (Onfi), oxazepam, and prazepam. The benzodiazepines are prescribed mainly for anxiety disorders, insomnia, and seizures, and their long-term use often leads to addiction. Moreover, they are depressant drugs, and their easy accessibility from shady pharmaceutical stores made them potential choice for sexual predators. Therefore, fast, selective and sensitive detection of such contraband would lead to a lowering of the DFSA incidents.

4.1. Benzodiazepine sensors based on fluorescent metal complexes

Unlike GHB and ketamine, the benzodiazepine class of illicit drugs appeared much later in the streets, and hence, the

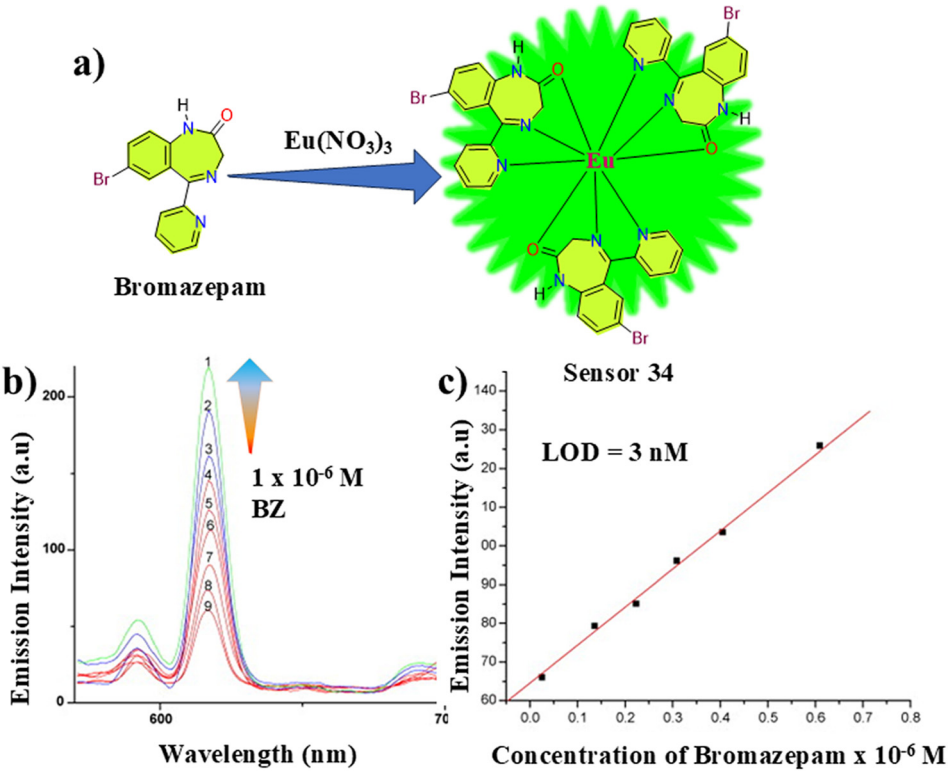

Fig. 16 (a) Synthetic scheme of sensor **34**, (b) luminescence enhancement of sensor **34** with increasing concentration of bromazepam, and (c) limit of detection of bromazepam from emission titration. Reprinted with permission from ref. 54. Copyright 2009, Elsevier B.V.

development of fluorescent sensors is only in their nascent phase.

The first example of bromazepam estimation using Eu(III) sensitisation was reported by M. S. Attia in 2009.[54] The bromazepam, owing to the presence of multiple coplanar coordination sites was proposed to behave as an antenna for the lanthanide sensitisation in the Eu(III) bromazepam complex **34**, leading to a simple but effective sensing strategy. Bromazepam was procured commercially and was ground for prompt solubilisation in ethanol. When the Eu(III) stock solution was slowly added to the sensor, the two absorption peaks of the free sensor at 251 and 328 exhibited a hypsochromic shift of 7 nm. The as-formed metal complex furnished a sharp emission at 617 nm upon excitation at 390 nm (Fig. 16b). Using different variables such as pH, Eu(III) and bromazepam concentration, it was observed that within 10 minutes of mixing and 1 : 2 ligand-to-metal ratio, it obtained maximum emission output. Optimal sensing occurred at pH 7.4 in phosphate buffer, with the intensity stable for 2 hours. The method offered excellent sensitivity, with linearity from 2.3×10^{-8} to 6.2×10^{-7} M. The complex formation experiment with changing metal ion concentration established a detectable limit of 3 nM for the bromazepam. Solvent-dependent photophysical analysis revealed emission quenching in protic solvents (water and ethanol) but retention in aprotic media (acetonitrile and DMF). The probe was validated using commercial tablets (Bromazepam, Calmepam, and Clopam) and in spiked serum samples, showing recoveries ranging from 101.2 to 102.2 with a relative standard deviation (RSD) of ~0.44%, demonstrating high accuracy when compared with British Pharmacopoeia LC methods. The main strengths of this method are its simplicity, sensitivity, and ability to work in real samples. However, drawbacks include reliance on Eu^{3+} lanthanide salts, need for aprotic solvents, and applicability limited mainly to bromazepam, not the full benzodiazepine group of drugs.

Although the aforementioned report was the first example of lanthanide-sensitized fluorescence sensing, the long complexation time, solvent dependency, and possible interference from other chelating agents in street drugs require a more sophisticated approach towards sensing. In this regard, Kong and coworkers have come up with a new Eu-MOF for the sensitive detection of flunitrazepam.[55] Using 1,3,5-benzenetricarboxyllic acid as a framework expander, 1,10-phenanthroline as a sensitiser and Eu(III) as the metal centre, the Eu-MOF **35** was prepared *via* a solvothermal method (Fig. 17a).

The Eu MOF **35** was ground and suspended in a methanol–water system at 150 °C for 12 hours, producing a stable crystalline framework with a BET surface area of 131 $m^2\ g^{-1}$ and mesoporous channels with a diameter of approximately 18 nm. Upon excitation at 284 nm, the probe emitted intense red luminescence at 615 nm, arising from the $^5D_0 \rightarrow {}^7F_2$ transition of Eu^{3+}, enhanced by an efficient "antenna effect" from both the ligands.

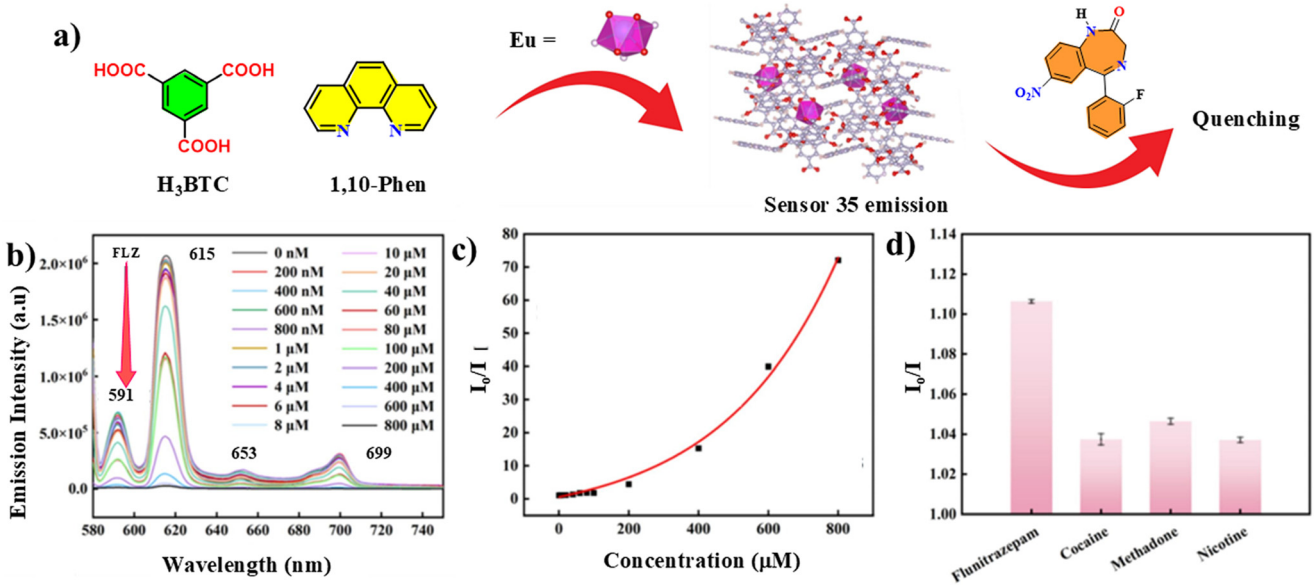

Fig. 17 (a) Schematic of the preparation and sensing of the sensor **35**, (b) fluorescence titration with flunitrazepam, (c) Stern–Volmer plot, (d) LOD determination from emission titration and (d) selectivity in the presence of interfering narcotics. Reprinted with permission from ref. 55. Copyright 2025, Elsevier B.V.

When a flunitrazepam solution was incrementally added to the suspension, the emission of both the peaks displayed a gradual quenching. With the increase in analyte concentration to 800 μM, a maximum 98.6% quenching was observed along with a very low limit of detection of 73 nM. The authors investigated the quenching mechanism using theoretical calculations and attributed the sharp emission loss due to a combination of photoinduced electron transfer (PET) and an inner-filter effect (IFE), where the drug's low-lying LUMO level (−2.68 eV) accepted electrons from the excited Eu-MOF. The material maintained high luminescence stability across solvents and temperatures, and was successfully applied to real urine and beverage samples, showing excellent reproducibility (RSD ≈ 2.5%) and a clear visual colour change under UV light (365 nm) when immobilized in an agarose matrix. These results confirmed the Eu-MOF's potential for *in situ*, rapid forensic screening of flunitrazepam without sophisticated instruments. However, the probe's methanol-dependent operation, high-temperature solvothermal synthesis, and the turn-off sensing mode, which

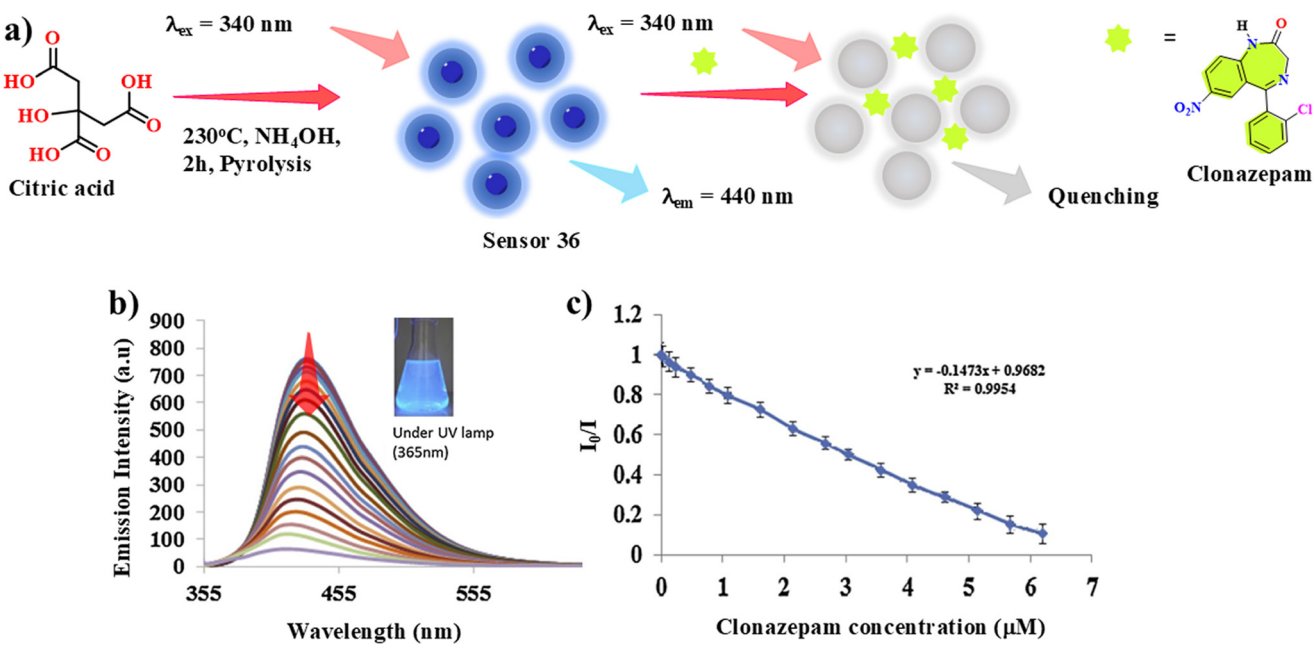

Fig. 18 (a) Synthetic scheme and sensing behaviour of **36**, (b) fluorescence titration of sensor **36** with clonazepam, and (c) limit of detection from titration measurements. Reprinted with permission from ref. 56. Copyright 2020, Elsevier B.V.

can be affected by background quenching in complex matrices, limit its practical application.

4.2. Fluorescent nanomaterial sensors for benzodiazepines

As previously discussed, the organic small molecule and metal-based sensors are expensive, leave a permanent environmental impact, and are sometimes difficult to scale up, which leads to poor viability towards commercialization. The nanomaterial-based sensors, however, provide all the necessary traits along with similar selectivity, sensitivity and easy preparation. Considering this usefulness in mind, Hamisekhar *et al.* have reported a new luminescent nitrogen-doped carbon nanodot for the sensing of clonazepam.[56] The carbon dot (CD)-based sensor **36** was prepared *via* the pyrolysis of citric acid, and ammonia was used as the source of doped nitrogen (Fig. 18). The formation of the CDs was further investigated using nano characterisation techniques such as DLS and TEM, yielding spherical particles with a diameter between 3 and 9 nm with abundant surface-bound hydroxyl, carboxyl, and amine groups. For photophysical experiments, the CDs were suspended in a PBS buffer, and strong absorption peaks were found at 230 and 327 nm, which were attributed to π–π* and n–π* from C═C and C═O transitions, respectively. When excited at 340 nm, a strong blue emission peak at 440 nm appeared, indicating the discernible optoelectronic capacity of the CDs. When a methanolic clonazepam solution was added to the CD suspension, the blue emission gradually decreased with a minor 17 nm hypsochromic shift at the end, highlighting strong fluorescence quenching tendency of the analyte. By comparing with the previous results, the exploration of the analyte structure helped the authors to deduce that the binding of clonazepam with electron-deficient nitro functional groups altered the energy migration dynamics of the sensor, leading to the depleted emission. To evaluate the sensitivity of the sensor **36**, fluorescence titration was carried out with different analyte concentrations and a very low limit of detection of 12 nM was obtained.

The highly sensitive nano materials were further exposed to different interfering entities such as cations, amino acids, sugars and other benzodiazepine analogues such as lorazepam and alprazolam, and no observable change in the emission was visible, indicating high selectivity of the sensor towards clonazepam.

pH optimization showed stable sensing capacity between pH 4 and 10, and the measurements were carried out at pH 6.8 in a phosphate buffer. Selectivity tests against other benzodiazepines, common cations, and biomolecules showed negligible interference. Real sample validation in human plasma and pharmaceutical tablets demonstrated recoveries between 95 and 105% with RSD values <5%. The main limitation of the sensor **36** was the reliance on the instrumental fluorescence readout (not naked-eye), so it was less suited for rapid consumer-level field testing while excellent for laboratory or clinical settings.

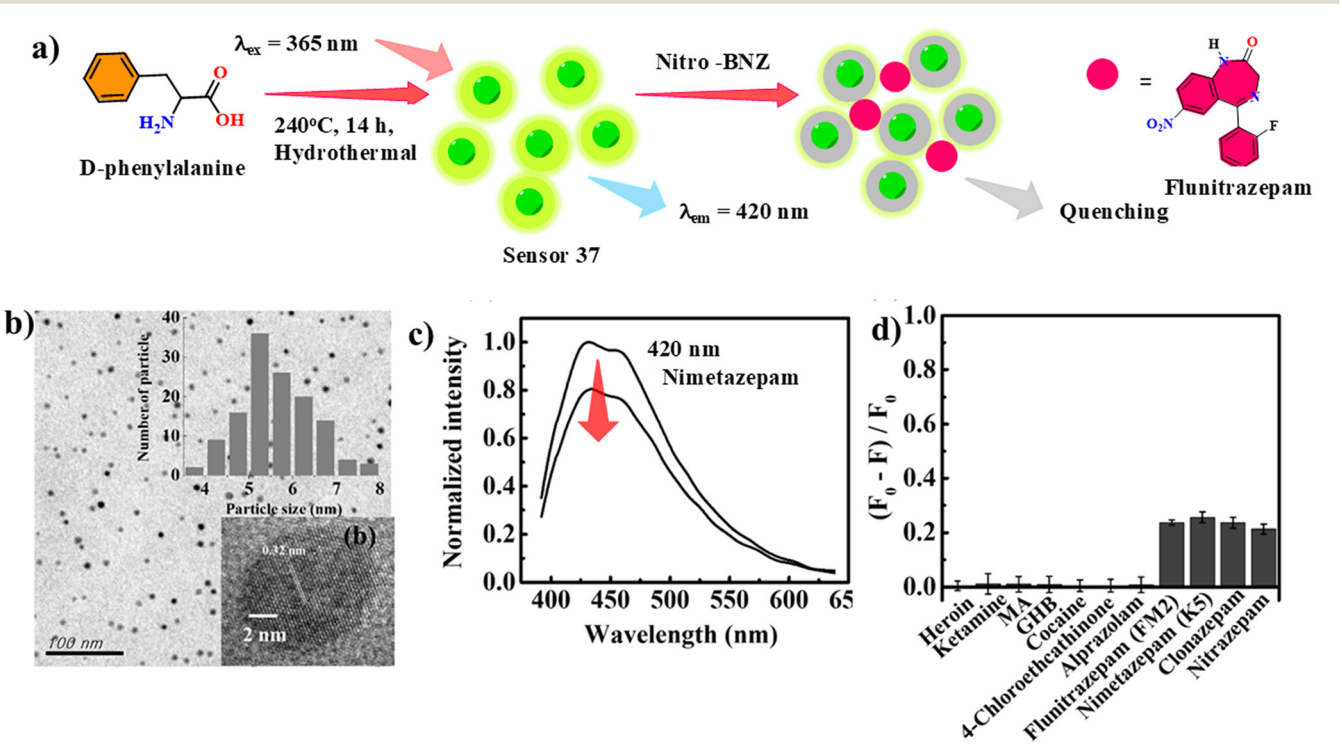

Fig. 19 (a) Hydrothermal preparation of sensor **37** from amino acid, (b) TEM analysis of the nanoparticles, (c) luminescence quenching of sensor **37** upon the addition of nimetazepam, and (d) selectivity towards nitro-containing benzodiazepines. Reprinted with permission from ref. 57. Copyright 2020, Elsevier B.V.

Based on the nanomaterial platform, Ten and Chang proposed the preparation of a hydrophobic carbon dot-based sensor **37**.[57] The authors argued that due to poor solubility, the benzodiazepine employs weak interaction with the sensors in aqueous conditions, and thus, a hydrophobic sensor would resolve the issue and furnish much higher sensitivity. Using a hydrothermal route, the sensor **37** was prepared from phenylalanine suspended in toluene. The as-prepared sensor **37** was purified, dried and resuspended in a mixture of ethyl acetate and dichloromethane and subsequently characterised using IR, UV, fluorescence, Raman, TEM and XPS (Fig. 19b). During optical experiments, a broad absorption peak at 365 nm was found along with a similar wide emission maximum at 430 nm, indicating emission in the blue region of the visible wavelength. For the hydrophobic interaction experiments with the benzodiazepine analogues, a toluene suspension of the sensor was exposed to different concentrations of nimetazepam, which led to a steady quenching of the emission. Analysis of the calibration curve established the limit of detection as 7.24 μM, which indicated the very strong sensitivity of the sensor **37** towards the analyte. When different nitro benzodiazepines such as clonazepam and flunitrazepam were used in combination with ketamine, cocaine, GHB, *etc.*, similar quenching responses were obtained, indicating a broad substrate scope of the sensor. The mechanistic analysis indicated unperturbed absorption spectra, which rules out any possibility of ground-state complex formation and further theoretical estimation of the energy level indicated photoinduced electron transfer between the sensor and the analyte.

As previously discussed, compared to simple fluorescence on or off signalling, the ratiometric sensor provides additional advantages such as negation of background interference and higher sensitivity. Therefore, Soleymani *et al.* have developed a ratiometric fluorescence and internally calibrated polydopamine nanoprobe **38** for the selective detection of clonazepam.[58] To afford the nanoparticle, commercially procured dopamine was dissolved in tris(hydroxymethyl)aminomethane hydrochloride. Ethylene diamine was subsequently added to suppress the surface π–π* interaction, thereby enhancing the radiative emission. The polydopamine nanoparticle furnished only a single emission peak at 475 nm, but to induce a ratiometric response red-emitting rhodamine B (RhB) was incorporated as an internal calibration and a non-interacting member with emission maxima at 570 nm. For the sensing experiment, the change in the ratio of these two peaks, along with the changing analyte concentration was used to validate the sensitivity. When clonazepam was gradually introduced to the suspended sensor, the nanoparticle emission at 475 steadily increased, whereas the RhB peak remained unchanged. The authors proposed that due to the presence of nitro groups of the analyte, it disrupted the detrimental π–π* energy loss of the

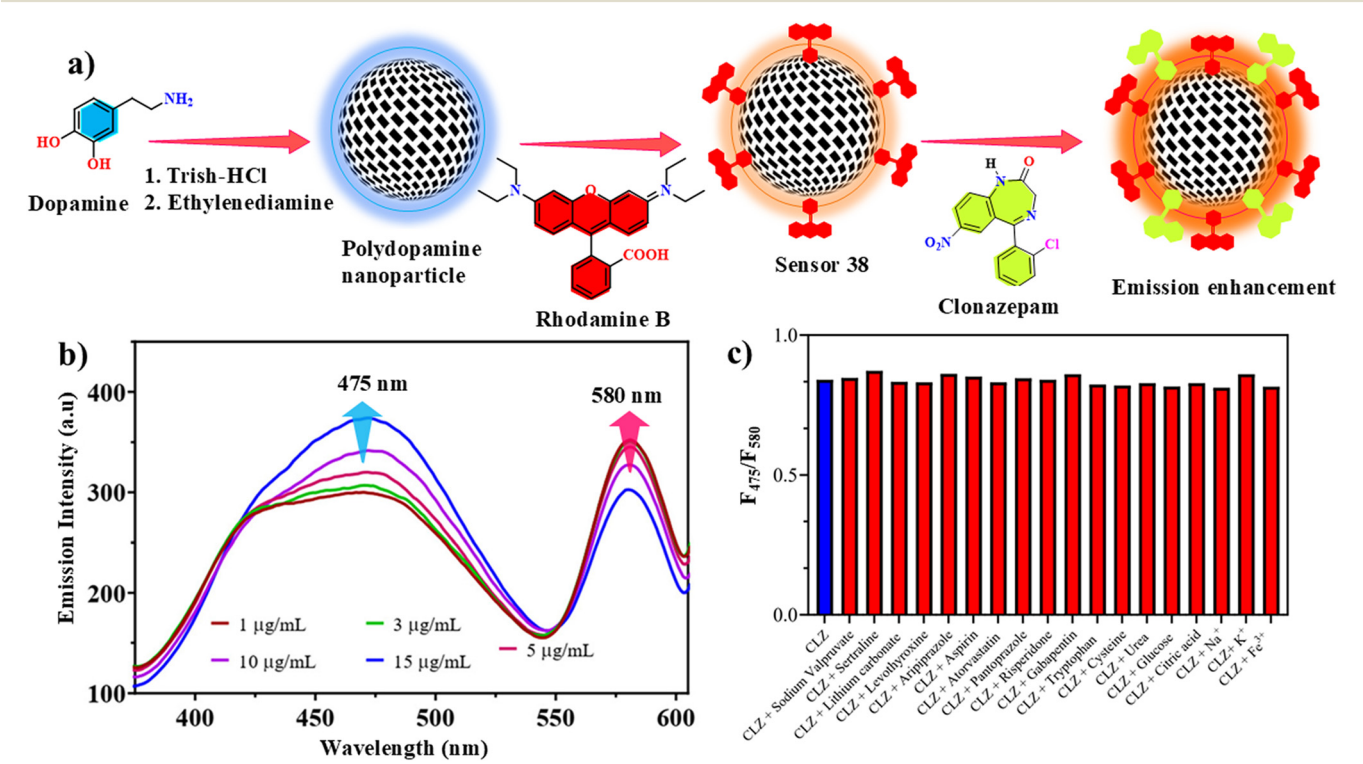

Fig. 20 (a) Preparation of rhodamine–polydopamine nanoparticle composite, (b) change in the emission profile of sensor **38** with increasing clonazepam concentration, and (c) effect of interfering additives on the ratiometric response of sensor **38**. Reprinted with permission from ref. 58. Copyright 2024, Wiley VCH GmBH.

sensor, leading to enhanced emission. The RhB has no affinity towards clonazepam, and the emission was unaffected (Fig. 20). When the LOD was estimated using the altered ratio of the emission peaks with respect to varying analyte concentration, 15.87 nM was found which was substantially low compared to the previously developed sensors. The method was optimized at pH 2.5 in Tris–HCl buffer, requiring only a 1 minute incubation, and showed high repeatability with recoveries of 81–105% and RSD $<$ 10%. Most importantly, the system remained stable for up to 48 hours, exhibiting excellent selectivity even in the presence of common biological interferents such as amino acids, ions, and co-administered drugs. When applied to real patient plasma, the probe successfully quantified clonazepam levels between 0.007 and 0.097 μg mL^{-1}, comparable to HPLC results, confirming its analytical reliability. Despite these strengths, the approach required acidic media for optimal signal response and acetonitrile pretreatment for protein removal, which may hinder practical applications. Moreover, long-term nanoparticle stability beyond two days remained uncertain.

The quantum dot, which is the inorganic analogue of the conventional carbon dot, furnishes several superior emission characteristics such as no energy loss from π–π* interaction, controllable and tuneable sharp emission, and higher shelf life. Considering all these advantages, Malekaneh and coworkers have developed Mn-doped ZnS luminescent quantum dots.[59] To tune in the selectivity and sensitivity, the QDs were decorated with a molecularly imprinted polymer using methacrylic acid as a building unit *via* a non-invasive photopolymerization. To induce selectivity, diazepam monomer was used as a template in the polymer imprinting process. The formation of the MIP-coated QD-based sensor **39** was established using a range of analytical tools, such as FT-IR spectroscopy, as well as TEM (Fig. 21).

The sensor **39** furnished a strong emission peak at 590 nm upon illumination at 320 nm. The authors selected diazepam as the substrate, and the addition of the analyte induced a steady reduction of the emission intensity. From the fluorescence quenching experiment, the limit of detection was determined as 87.8 nM. Due to the use of diazepam in the imprinting process, the QDs were highly selective when exposed to other analogous substrates.

Sensor **39** showed excellent photostability and reproducibility, with recoveries between 93.6% and 100.2% and RSD values below 8% in tablet and human serum samples. Interference studies indicated strong selectivity for diazepam and its metabolites, with minor cross-reactivity toward oxazepam, lorazepam, and nordazepam, while inorganic ions had negligible influence when standard-addition calibration was applied. The study concluded that coupling the optical sensitivity of Mn-doped ZnS QDs with the molecular recognition of MIPs produced a low-cost, sensitive, and reproducible nanosensor for pharmaceutical and biological analyses.

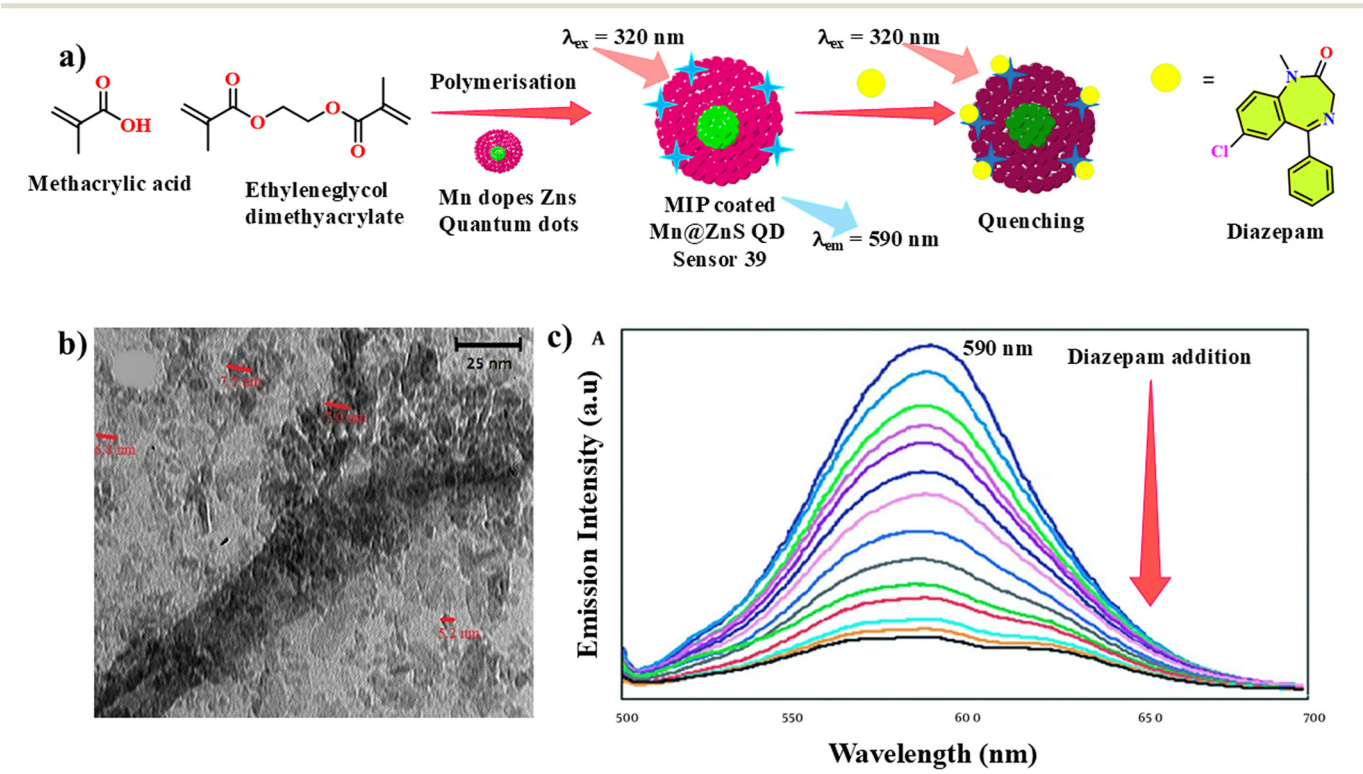

Fig. 21 (a) Schematic of the preparation of sensor **39**, (b) TEM image of **39**, (c) change in the luminescence profile of sensor **39** with the addition of diazepam. Reprinted with permission from ref. 59. Copyright 2022, Abdolraouf Samadi-Maybodi.

5. Detection of ketamine by fluorescence sensing process

Ketamine, which is derived from phencyclidine, is often used for the treatment of pain and depression, but with a higher dose, it can induce amnesia, hallucination, sedation, *etc.*, and can even be lethal. Being one of the most promising choices for the perpetrators of DFSA, it is one of the newest additions to the long list of narcotics. And hence, development of a fast and reliable ketamine sensor is of utmost importance.

5.1. Organic small molecule-based fluorescent ketamine sensors

Compared to the conventional GHB and benzodiazepine group of narcotics, which were known for their clandestine use, ketamine was mainly applied for pain management, and it gradually gained prominence for illegal application. Therefore, research on fast and efficient detection of ketamine is still in the nascent stage. The liquid ketamine is often solidified by transforming into a corresponding hydrochloride salt for the ease of transportation, procurement, and use. Thus, along with the liquid phase detection, it is of utmost importance to have access to sensors with solid-state detection capability.

Cheng and Fan have reported a carbazole–fluorene conjugate sensor **40** as the first solid-phase luminescent sensor for ketamine.[60] The target molecule was prepared using multistep reactions and purifications to afford the final compound as a white solid, which was thoroughly characterised with various analytical techniques such as NMR, IR, UV, mass spectrometry, and most importantly, by single-crystal XRD analysis.

The optoelectronic investigation of the sensor in THF revealed absorption and emission at 375 and 398 nm, respectively. When a thin film was prepared using a drop-cast method on Whatman filter paper, the UV and fluorescence maxima shifted to 339 and 463 nm, correspondingly (Fig. 22c). Such bathochromic and hypsochromic shifts in photophysical properties are often associated with the formation of aggregates upon solidification. The morphological evaluation of the thin film using SEM analysis supported the existence of spherical particles with an average diameter ranging from 150 to 350 nm.

When the thin film of sensor **40** was exposed to aqueous ketamine, the major peak at 463 remained unperturbed, but a new peak at 398 appeared. The intensity of the new peak gradually increased with different analyte concentrations and increased by a maximum of three-fold with 0.1 M mL^{-1} ketamine concentration. A sensor film was able to furnish a detectable emission profile at a bare minimum of 0.04 μM of ketamine, which pushed the analyte boundary to 50 pg cm^{-2} on the film.

Apart from the solid-phase sensitivity, for selectivity evaluation, when the effect of other solid narcotics and household white chemicals were analysed, only methylamphetamine furnished comparable luminescence enhancement.

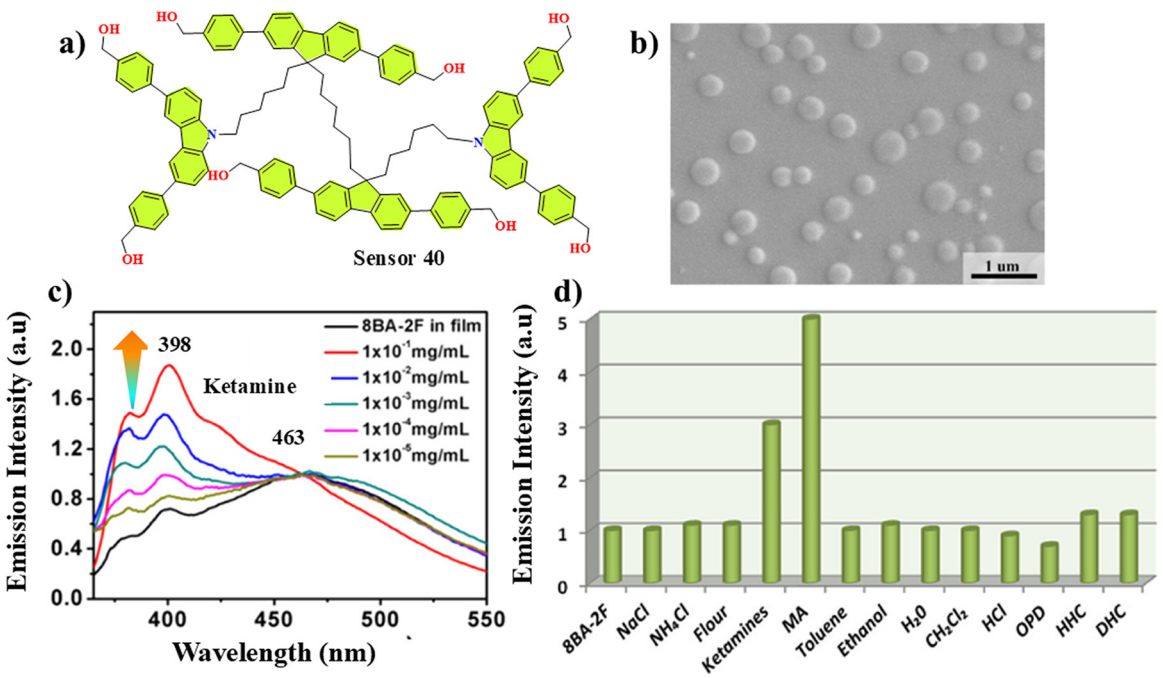

Fig. 22 (a) Molecular structure of sensor **40**, (b) SEM image of the sensor **40** thin film, (c) fluorescence enhancement with varying ketamine concentrations, and (d) selectivity of the sensor towards other narcotics. Reprinted with permission from ref. 60. Copyright 2016, the American Chemical Society.

Theoretical calculations revealed that strong hydrogen bonding between –PhCH$_2$OH groups and the protonated –NH$_2$ sites of the drugs, along with hydrophobic and electrostatic interactions, reduced the aggregation of sensor **40** and altered the molecular torsion angles, causing fluorescence enhancement at 398 nm. No photoinduced electron transfer (PET) was possible since the LUMO levels of ketamine lay below those of the sensor. The overall mechanism was attributed to aggregation disruption and steric configuration change rather than redox quenching. The system requires a short drying step and UV excitation, and it only functions in thin-film contact mode, limiting solution-phase versatility. Nevertheless, it represents the first picogram-level, naked-eye, solid-state probe for ketamine, offering a low-cost, reagent-free, and portable approach for real-time on-site detection. Although highly practical, this design was limited to surface detection and lacked quantitative precision, prompting further exploration into biomolecular and nanoscale systems capable of selective, quantitative analysis in biological fluids.

The solid-state emission profile was mostly attributed to the aggregated form of the sensor, and following the similar trend, Hu and coworkers have developed a new cucurbit mediate AIE sensor **41** for the detection of trace amounts of ketamine in solutions.[61] The authors observed that the addition of non-fluorescent alkaloid palmatine to cucurbit[8]uril created a highly emissive host–guest complex sensor **41**. Careful investigation with ^{1}H NMR established that two palmatine guests are oriented in close proximity in the host, resulting in a strong aggregation-induced emission (Fig. 23a). The authors proposed that due to weak host–guest interaction, when treated with analytes with a higher binding affinity towards cucurbit[8]uril, it can undergo host displacement and emission changes. Therefore, the (palmatine)$_2$@cucurbit[8]uril or sensor **41** was treated with different narcotics and distinguishable changes were observed for the date rape drug ketamine.

The host–guest complex in water furnished strong emissions at 540 nm when excited at 370 nm. For the sensitivity analysis, the ketamine-induced emission studies were executed in a PBS buffer mimicking the physiological conditions. With the increase in the amount of ketamine, the emission of the sensor **41** steadily decreased, and the author proposed the guest displacement as the possible reason. When the guest displacement was analysed with proton NMR studies, noticeable changes were obtained for the ketamine aromatic and amine protons. The protons of the aromatic ring of the ketamine furnished up-field shifts indicating shielding by the aromatic rings of the host and the palmatine protons moved lower de shielded zone after displaced by the analyte. The host–guest complexation resulted in a very low limit of detection of 21 nM, indicating high sensitivity. For selectivity analysis, a wide range of illegal street drugs such as cocaine, heroin, fentanyl, and alprazolam were subjected to exposure of sensor **41** and only a noticeable change was induced by ketamine. For practical applications, ketamine-spiked urine samples were subjected to photophysical analysis, where recovery values ranging from 96.1

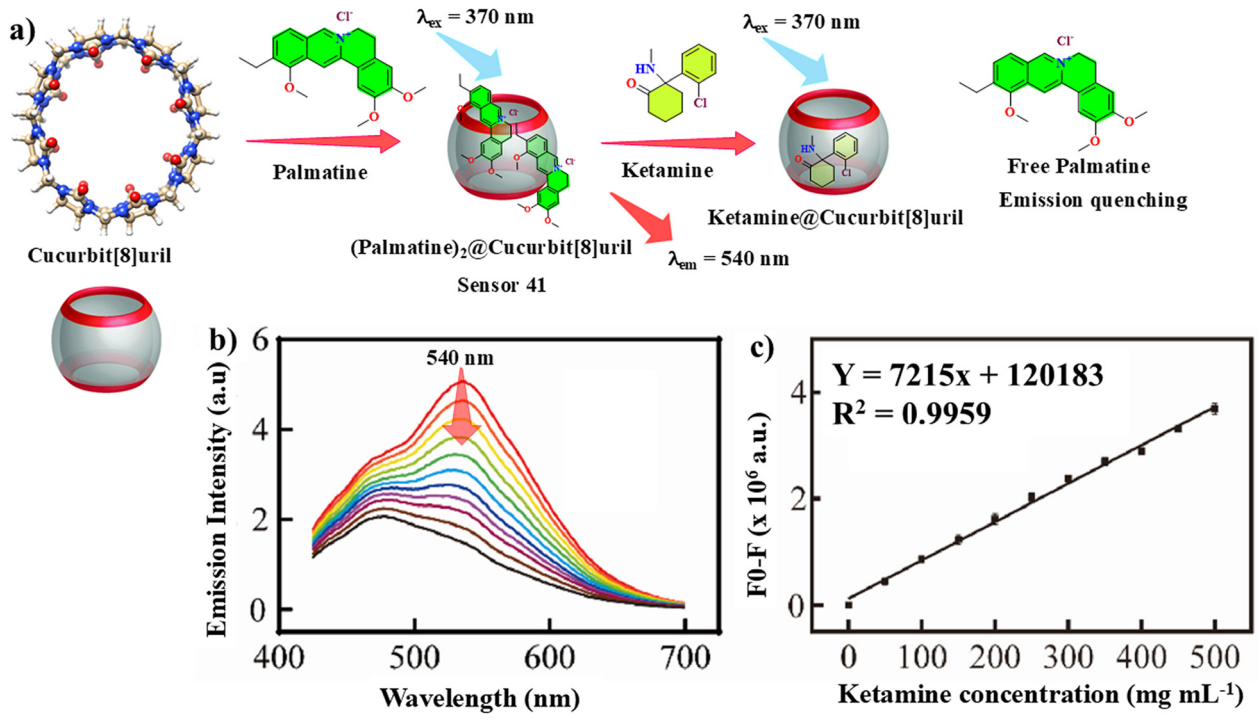

Fig. 23 (a) Palmatine-cucurbit[8]uril host–guest complex formation, (b) fluorescence titration of sensor **41** with ketamine, and (c) limit of detection of analyte from the fluorescence titration experiment. Reprinted with permission from ref. 61. Copyright 2022, Elsevier B.V.

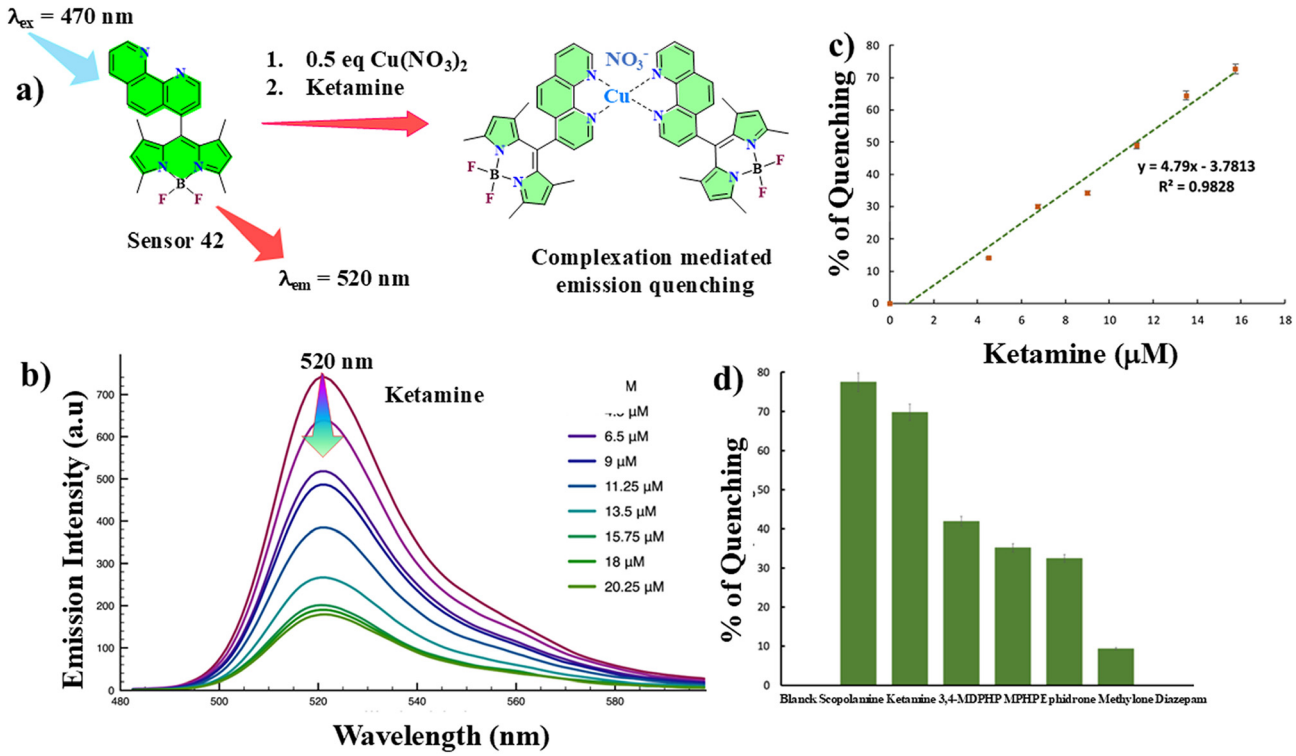

Fig. 24 (a) Complexation-induced emission quenching of sensor **42**, (b) effect of increasing ketamine concentration on the emission of sensor **42**, (c) limit of detection from the emission quenching, and (d) interference of other narcotics on the sensing behaviour of **42**. Reprinted with permission from ref. 62. Copyright 2024, Elsevier B.V.

to 103.9% were obtained, indicating strong sensitivity towards the analyte.

Gavina, Saez, and others have reported the first fluorescent sensor **42** for the detection of ketamine as well as scopolamine based on a BODIPY scaffold.[62] The authors have previously developed a range of cathinone class of drug sensors by using their chemical reduction of Cu(II) complexes to Cu(I) complexes. For the current strategy, they combined a BODIPY building unit and covalently attached 1,10-phenanthroline as the metal chelator. The sensor was synthesized in two steps: the oxidation of 4-methyl-1,10-phenanthroline to its aldehyde, followed by condensation with 2,4-dimethylpyrrole and boron complexation to form the BODIPY-Phen dye. Structural analysis by single-crystal X-ray diffraction confirmed an orthorhombic lattice with a nearly planar BODIPY core and a perpendicular phenanthroline ring (98.30° dihedral angle), ideal for metal coordination.

Photophysical characterisation revealed strong absorption bands at 507 with smaller shoulders at 476 and 270 nm and a single emission peak at 520 nm. BODIPY-derived fluorophores are well known for sharp peaks and a smaller Stokes shift. For the sensing experiments, when equimolar Cu(II) was added, no significant change occurred for sensor **42**, but the subsequent introduction of ketamine induced intense fluorescence quenching and a visible colour shift from pale green to brown-pink (Fig. 24). The response, optimized at 10 min and 60 °C, was attributed to the reduction of Cu(II) to Cu(I) by the amine-containing drug, followed by Cu(I) coordination to the phenanthroline moiety, disrupting BODIPY emissions through a redox-driven turn-off mechanism. UV-vis titration confirmed the formation of a 2 : 1 ligand-to-Cu(I) complex, consistent with the observed spectral changes.

The limit of detection for ketamine estimated from the fluorescence titration plot was found to be 2.88 μM. Moreover, the sensor **42** was found to be unresponsive towards common interfering ingredients obtained in commercial drinks such as tartaric acid, sucrose, and sodium ascorbate, as well as other addictive paraphernalia such as diazepam and methylone. The sensor **42** offered a fast, inexpensive, and portable fluorescence-colorimetric platform for detecting DFSA-related drugs. However, its micromolar sensitivity and temperature dependence suggest that further work is needed to improve ambient-condition performance and adapt the design toward biological samples. Nonetheless, this work marked a significant advance in metal–organic optical probes for field identification of DFSA-related drugs.

5.2. Fluorescent nanomaterials for ketamine detection

Compared to the small molecules and metal complex-based luminescent sensors, the nanomaterial-based ketamine sensors furnish additional advantages such as easy synthesis and purification, high sensitivity due to more surface area, and ease of fabrication. Considering the aforementioned advantages of nanomaterials, Zha *et al.* demonstrated a DNA-

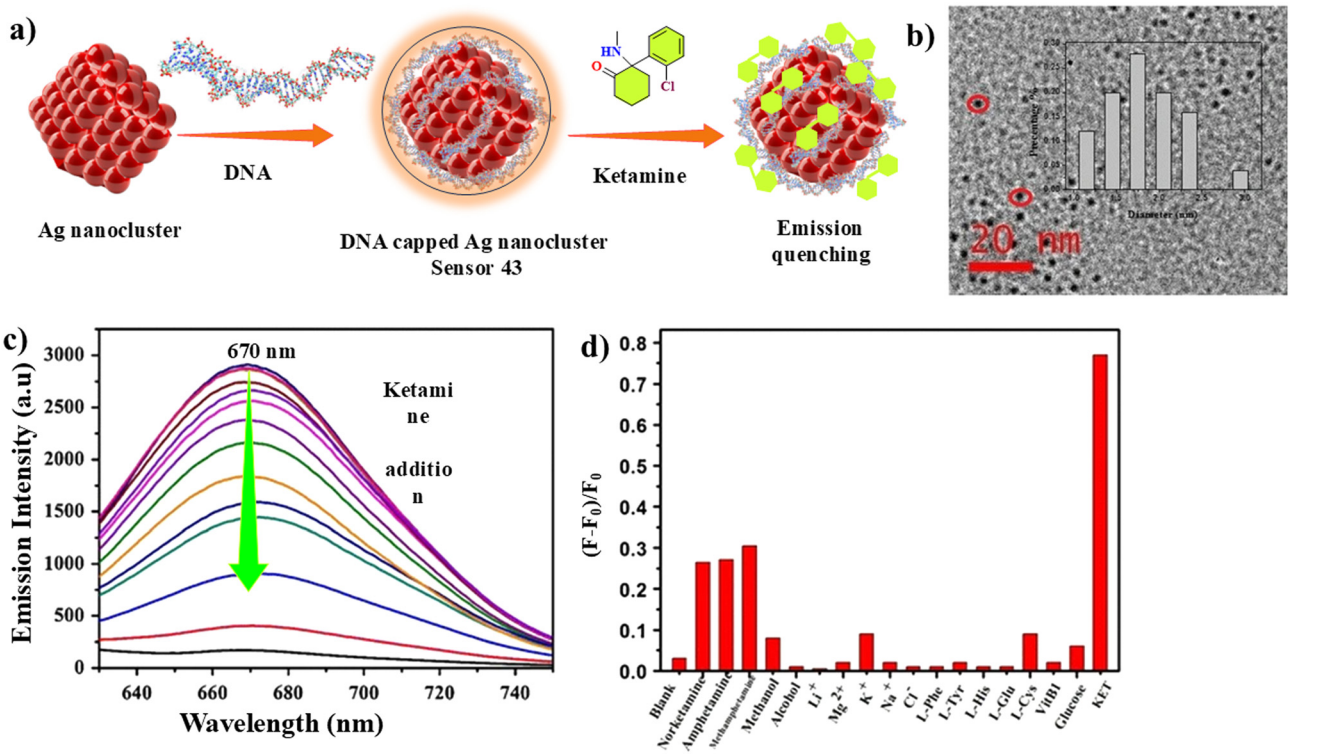

Fig. 25 (a) DNA templation and ketamine sensing of sensor **43**, (b) TEM images of the nanocluster, (c) luminescence quenching upon ketamine addition, and (d) selectivity of sensor **43**. Reprinted with permission from ref. 63. Copyright 2002, Springer Nature B.V.

Ag nano cluster sensor **43**. The authors decorated a luminescent Ag nanocluster with a suitable DNA fragment where one half was designed as the capping agent to stabilise the nanocluster, whereas the remaining half had a history of strong ketamine affinity.[63] The as-prepared DNA-Ag nanocluster formation was investigated with TEM measurement, revealing spherical-shaped particles with an average diameter of 1.75 ± 0.3 nm (Fig. 25b). The photophysical studies furnished a pair of absorption peaks at 350 and 430 nm, whereas a wide emission maximum at 670 nm appeared when excited at 600 nm. As suggested by the author, a part of the DNA had a strong affinity towards ketamine, and when the analyte was gradually added to the nanocluster, the emission profile steadily decreased. Upon ketamine addition, the fluorescence was quenched from 2800 au to about 1970 au, originating from complex structural rearrangement and binding of ketamine to the recognition region. The optimized sensing conditions included pH 7.0 (physiological medium) and a 4 min incubation time, producing maximal and stable quenching. The very small quantity of the ketamine required to quench the emission intensity is also reflected in the limit of detection, which was found to be as low as 0.25 nM, indicating the very high sensitivity of the sensor **43**. Selectivity studies showed negligible interference from alcohols, amino acids, vitamins, and common ions; only structurally related amines such as norketamine and amphetamine produced partial responses. The sensor accurately quantified ketamine in spiked and forensic blood samples with RSD $< 10\%$, in close agreement with the GC–MS results (relative deviations 5.4–8.5%). This DNA-AgNC genosensor offered a simple, rapid, and highly sensitive approach for direct blood analysis, representing the first demonstration of a fluorescence genosensor for ketamine suitable for forensic and clinical screening.

Although the Ag nanocluster **43** demonstrated strong ketamine affinity, selectivity, and sensitivity, their poor photostability, DNA fragility, and cold-storage dependence were critical issues that plagued the potential for practical application. Moreover, the luminescence enhancement is much more informative and accurate than emission quenching.

Considering all these advantages in mind, Liu and Chen reported a new fluorescein-attached DNA-capped Au nanosphere sensor **44**.[64] The Au nanomaterial is protected by the DNA, which further acts as a bridge between the fluorescein and the nanosphere. The formation of the nanoparticle was thoroughly characterised using various nano-analysis techniques, and the TEM images suggested the formation of a spherical Au nanoparticle with an average size of 13 ± 2 nm. Moreover, the sensor was found to be completely non-emissive when excited at 490 nm, and the author ascribed the energy loss to FRET from fluorescein to the Au nanosphere. The probe was constructed by functionalizing AuNPs with a Y-shaped DNA (Y-motif) that carried the ketamine-binding aptamer. When ketamine was added along with the ds-DNA, the U-DNA underwent

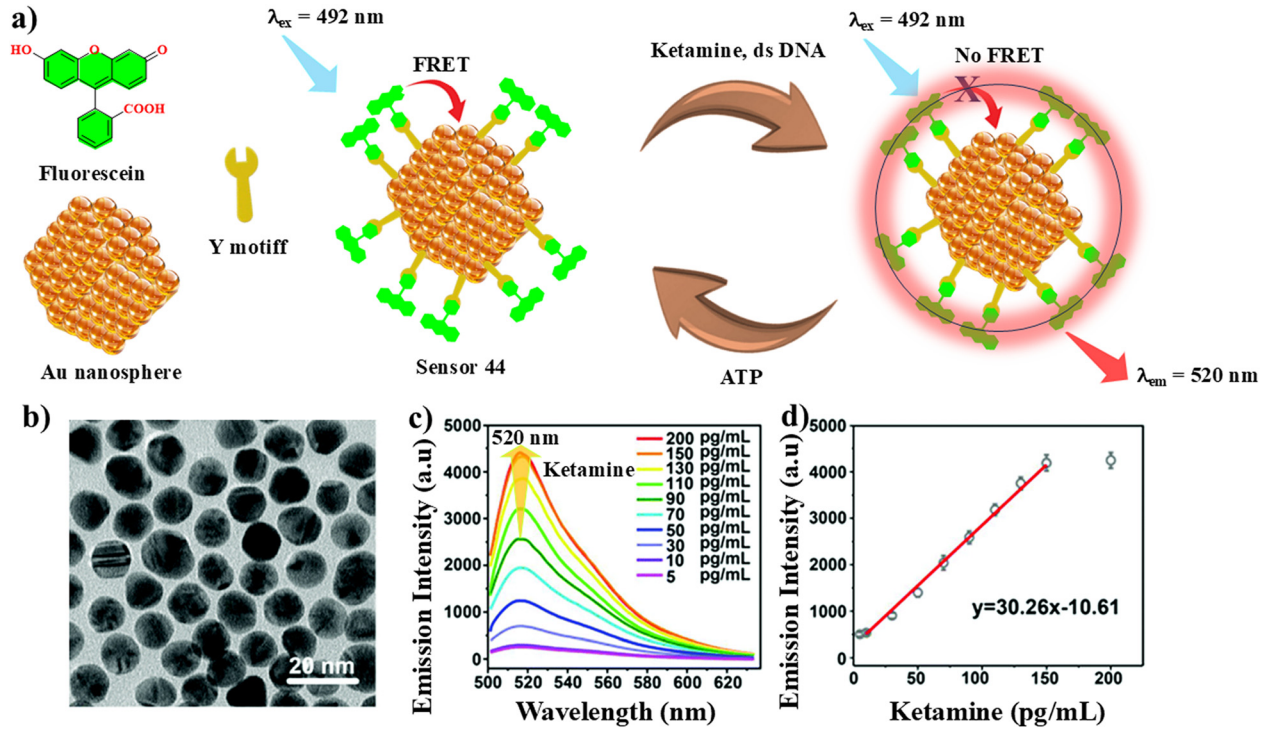

Fig. 26 (a) Schematic of the ketamine sensing of sensor **44**, (b) TEM image of sensor **44**, fluorescence titration (c) and limit of detection estimation (d) for sensor **44**. Reprinted with permission from ref. 64. Copyright 2019, the Royal Society of Chemistry.

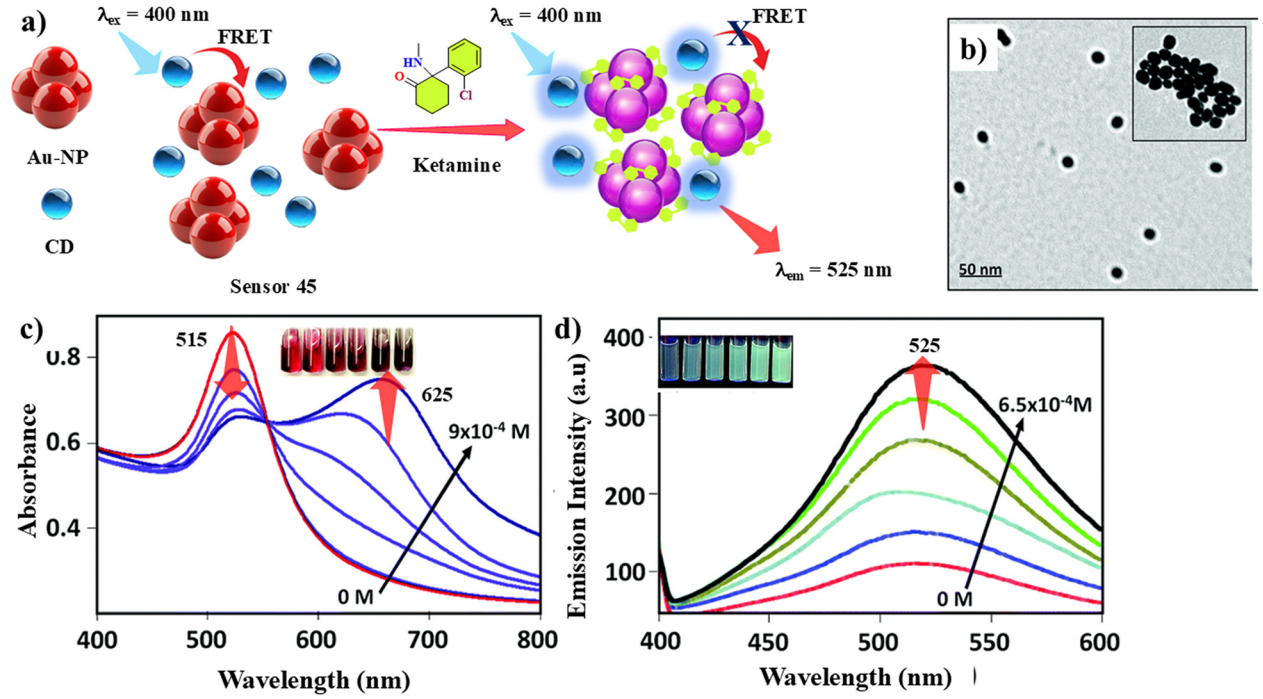

Fig. 27 (a) Ketamine-induced photophysical changes of sensor **45**, (b) TEM images of Au-NPs, and the change in the absorbance (c) and luminescence (d) of sensor **45** upon the addition of incremental amounts of ketamine. Reprinted with permission from ref. 65. Copyright 2020, the Royal Society of Chemistry.

reorganisation and the FRET was inhibited, leading to emission enhancement. Moreover, when ATP was added. It further fuelled the reorganisation of the Y-DNA, and the sensor **44** was regenerated reversibly. The freshly regenerated sensor **44** was subsequently interacted with ketamine, which led to further emission enhancement, and such cyclic and

reversible disassembly and reorganisation of the sensor led to steady emission amplification (Fig. 26). Such signal amplification resulted in a very low limit of detection of 12 nM which is the lowest value ever reported, indicating the sensor efficiency. While this approach enabled picogram-level detection, the relatively long incubation time (≈90 min) limited its suitability for rapid on-site testing.

Yehia and coworkers developed an economically more viable alternative carbon dot (CD)–gold nanoparticle (AuNP) conjugate as a ketamine sensor **45**, where the aforementioned FRET-based fluorogenic response was combined with a chromogenic response, leading to a dual-channel sensor.[65] The author judiciously selected the CD–AuNP pair as literature reports established that the Au-NP has a strong ketamine affinity, which is reflected in their chromogenic response, as well as has a strong tendency to quench the CD fluorescence *via* FRET. The authors proposed that in sensor **45**, the ketamine binding to the Au-NP would lead to a drastic structural change, which would disrupt the FRET from CD to the Au-NP. As a result, a strong fluorogenic response from CD would occur. The authors prepared the CD and Au-NP following well-established protocols, and their morphological analysis revealed average-sized particles with diameters of 8.44 and 13.73 nm, respectively (Fig. 27b). The photophysical evaluation furnished three absorption peaks at 270, 340 and 405 nm for CD, and upon excitation at the same, a wide emission peak centred around 525 nm appeared. On the contrary, the AuNP furnished strong absorbance at 520 nm, indicating favourable FRET from the CD. When they were combined in an equimolar ratio, all the paternal absorbance was retained, but the emission was quenched due to FRET. When ketamine was added, there was a visible colour change from red to purple, which was predicted due to strong binding between ketamine and the Au-NP of the sensor **45**. It was proposed that the amine functional group, owing to favourable electrostatic interactions, strongly binds with the Au-NP, leading to the agglomeration of the nanoparticle with an absorbance shift from 520 to 625 nm. Due to the large Stokes shift of 120 nm, the FRET process was disrupted, and the sensor **45** emission from the CD rapidly enhanced. Therefore, the sensor furnished both chromogenic response and fluorescence turn-on sensing capacity. The dual-responsive sensor exhibited a low limit of detection of 13 μM. For practical applications, the sensor was applied to ketamine-spiked non-alcoholic beverages, and a strong dual-mode response was retained.

The same research group formulated a trimodal sensor **46** based on the CD–AuNP nanomaterial for commercialization and on-spot detection. The authors combined a polyaniline nanoparticle (PAN) and basic Co $(SCN)_2$ as potentiometric and chromogenic response materials.[66] Ketamine, due to the presence of secondary amine groups, has a tendency to be positively charged at low pH, which can induce a distinguishable potentiometric response from negatively

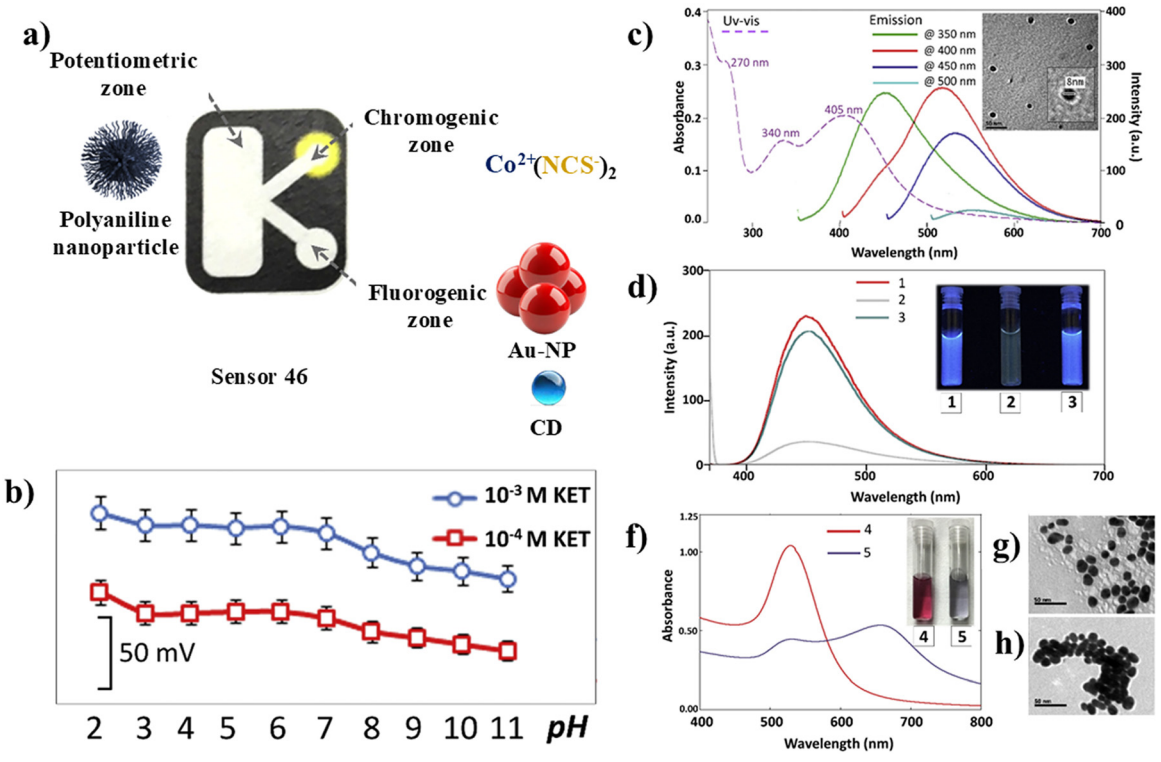

Fig. 28 (a) Design of the microfluidic sensor **46**, (b) potentiometric response of 46 towards ketamine, (c) excitation-dependent absorbance and emission of **46**, (d) emission profile of carbon dot, and sensor **46** before and after ketamine addition, (f) chromogenic response of sensor **46** towards ketamine and TEM images of sensor **46** before (g) and after (h) ketamine addition. Reprinted with permission from ref. 65. Copyright 2020, Elsevier B.V.

charged PAN. Moreover, in the presence of Co $(SCN)_2$ under basic conditions, ketamine forms a stable Lewis acid–base adduct, leading to a visible colour change, which is known as the Morris test and it is prominently used by narcotics and customs officers throughout the world. By judiciously combining the potentiometric, chromogenic and fluorogenic sensors on a paper, the authors fabricated the first known paper-based microfluidic trimodal ketamine sensor **46** (Fig. 28).

When different concentrations of ketamine solutions were added to the device, potentiometric changes were recorded, and the extrapolation of the linearly fitted data furnished a detection limit of 3.2 μM. The fluorogenic counterpart of the device furnished strong emission peaks at 453 and 519 nm when excited at 350 and 400 nm, respectively. From the previous discussion, it is evident that the binding of ketamine to the Au-NP led to structural changes in the nanoparticles, followed by the disruption of FRET, which culminated in strong emissions from the carbon dots. Finally, the Morris reagent changed the colour from blue to purple due to the change in the ligand environment of the Co^{2+} centre.

6. Conclusion

With the legalization of contrabands such as marijuana, and controlled distribution of narcotics, the current society has adopted a more lenient approach towards narcotics. Moreover, the involvement of organised crime syndicates and their clandestine cooperation have increased the distribution and outreach of such drugs into previously unexplored territories. The abuse of the contrabands not only increased the drug-related crimes but also affected the social stability and jeopardised public safety. Therefore, numerous analytical approaches such as spectroscopic, spectrometric, electrochemical, potentiometric, and immunosensing have been adopted for accurate and fast detection of such contrabands. More effort has been directed towards the detection and confiscation of potent substances such as cocaine, heroin, and amphetamines and the subtle counterparts such as date rape drugs are often overlooked. Unfortunately, with the more materialistic life approach, the drug-facilitated sexual predation is on the rise, and often they leave lasting physical and psychological trauma to the victim. In this regard, cheap, fast, and easy detection of such drugs is highly anticipated, and numerous fluorogenic sensors have been developed to accomplish this target. The luminescent sensors were built based on a myriad of platforms, including organic small molecules, polymers, metal-complexes, and nanoparticles, with each one of them providing unique advantages compared to others. Literature survey established a substantial number of reports on fluorogenic sensors of date rape drugs, but their substrate scope was either too specific or too generic, encompassing all types of contrabands. Herein, an attempt has been made to encompass all available luminescent sensors for all three major categories of date rape drugs. Although the sensors provided cheap, on-time sensing of controlled substances, often the results are incomplete due to poor bioavailability of the drugs, or influence of other interfering contrabands. Apart from aforementioned issues, the technical aspect of fluorogenic detection furnishes several concerning drawbacks. The luminogenic detection requires a handheld fluorimeter or a UV illumination device, which is more suitable for forensics but not for regular consumers; moreover, a minimum time is necessary to enforce sensor analyte interaction culminating in detection delay. Moreover, different analytes require different sensors, which makes it even more difficult to commercialise a universal sensor for all submission drugs. Thus, more extensive research is necessary to achieve a fast, universal, portable, and affordable sensor. Moreover, the vapor-phase detection of the analytes is more important than conventional solution-based sensors. Therefore, it is anticipated that, based on the current report, the development of more selective, biocompatible, fast and vapor-phase or solid-state fluorogenic sensors will be imminent.

Author contributions

Sunita wrote the original draft on the GHB section of the manuscript. Trisha and Dikshit wrote the original draft on the benzodiazepine and ketamine sections of the manuscript, respectively. Aniket conceptualized the work, worked towards funding acquisition, supervised the work and reviewed and edited the original manuscript.

Conflicts of interest

The authors declare that no personal or financial interests influenced the work reported.

Data availability

This review is a compilation of previously published works, and the reproduction of data and images was done with proper citation and permission from the authors and publishing houses.

Acknowledgements

The authors acknowledge the Department of Industrial Chemistry, Mizoram University, for providing research facilities. S. K., T. D., and D. B. also acknowledge Mizoram University for the MZU-UGC PhD Fellowship. S. K. also acknowledges INSPIRE for the Ph.D. Fellowship [DST/INSPIRE Fellowship/IF240221]. A. C. acknowledges the Science and Engineering Research Board for Start Up Grant [SERB/SRG/2021/000122] and the Royal Society of Chemistry for RSC Research Fund Grant [Grant No.: R24-8351624652].

References

1 United Nations Office on Drugs and Crime, *World Drug Report 2025*, United Nations Publication, Vienna, 2025.
2 D.-M. C. Anghel, G. V. Nitescu, A.-T. Tiron, C. M. Gutu and D. L. Baconi, *Molecules*, 2013, **28**, 4969.
3 *Drugs of Abuse Tests, United States Food and Drug Administration*, United States, 2023.
4 A. Lande, *The Single Convention on Narcotic Drugs*, International Organisation, Cambridge University Press, 1962, vol. 16, pp. 776–797.
5 United Nations Convention on Psychotropic Substances, United Nations Publication, Vienna, 1971, U.N. Doc. E/CN.7/AC.3/60.
6 T. D. Dillehay, J. Rossen, D. Ugent, A. Karathanasis, V. Vasquez and P. J. Netherly, *Antiquity*, 2010, **84**, 939–953.
7 M. Agarwala and C. Kulkarni, *Quat. Environ. Hum.*, 2024, **2**, 100032.
8 M. D. Merlin, *Econ. Bot.*, 2003, **57**, 295–323.
9 P. Teale, J. Scarth and S. Hudson, *Bioanalysis*, 2011, **4**, 71–88.
10 *European Drug Report 2024: Trends and Developments*, Luxembourg: Publications Office of the European Union, European Union Drugs Agency (EUDA), 2024.
11 C. Wei, X. Han, D. Weng, Q. Feng, X. Qi, J. Li and M. Luo, *Cell Discovery*, EUDA, 2018, vol. 4.
12 M. Chen, P. L. Burn and P. E. Shaw, *Phys. Chem. Chem. Phys.*, 2023, **25**, 13244–13529.
13 *The Social Impact of Durg Abuse, World Summit for Social Development*, United Nations Office On Drugs and Crime, 1995.
14 *Addressing Opioid Overdose Through Statewide Standing Orders for Naloxone Distribution*, Network for Public Health Law, 2019.
15 M. A. ElSohly and S. J. Salamone, *J. Anal. Toxicol.*, 1999, **23**, 141–146.
16 H. J. Farias and S. Reid, *Date-Rape Drug Prohibition Act of 2000*, Pub. L. No. 106–172, 2000.
17 M. Chen, P. L. Burn and P. E. Shaw, *Phys. Chem. Chem. Phys.*, 2023, **25**, 13244–13259.
18 M. Dagar, S. Yadav, V. V. S. Rai, J. Satija and S. Bhatia, *Talanta*, 2022, **238**, 123048.
19 K. Kim, S. Stoll, R. Singh, W. H. Lee and J.-H. Hwang, *TrAC, Trends Anal. Chem.*, 2023, **168**, 117295.
20 S. Soni, U. Jain and N. Chauhan, *Chin. J. Anal. Chem.*, 2021, **49**, 83–92.
21 N. Anzar, S. Suleman, Y. Singh, S. Kumari, S. Parvez, R. Piloton and J. Narang, *Biosensor*, 2024, **14**, 477.
22 E. Garrido, L. Pla, B. L. Torres, S. E. Sayed, R. M. Manez and F. Sancenon, *ChemistryOpen*, 2018, **7**, 401–428.
23 C. H. Chen, C.-C. Wang, P.-Y. Ko and Y.-L. Chen, *J. Food Drug Anal.*, 2020, **28**, 654–676.
24 S. Wei, Y. Li, H. Liang, Y. Yen, Y. Lin and H. Chang, *Anal. Sci.*, 2022, **38**, 247–260.
25 T. Dou, W. Yang, Z. Wang, J. Zhang, C. Yuan, J. Wang, Z. Xu, M. Zhang and D. Wang, *Small Methods*, 2025, 2500283.
26 A. Jangra, S. Chadha, H. Khajauri and R. K. Sarin, *J. Forensic Sci. Crim.*, 2021, **9**, 1–13.
27 Y. Mehta, S. Suleman, N. Anzar, R. Sharma and J. Narang, *Int. J. Environ. Anal. Chem.*, 2023, **105**, 372–393.
28 S. Chen, W. Huang, Y. Qiu, X. Zhang and J. Kong, *ChemistrySelect*, 2023, **8**, e202301659.
29 C. Yang, H. Yang, Z. Yao and T. Liu, *Analyst*, 2025, **150**, 1972–1985.
30 P. Anger, P. Bhardwaj and L. Novotny, *Phys. Rev. Lett.*, 2006, **96**, 113002.
31 A. Chowdhury, P. Howlader and P. S. Mukherjee, *Chem. – Eur. J.*, 2016, **22**, 1424–1434.
32 Z. Jiang, B. Wen, Y. Huang, Y. Wang, H. Fang and F. Li, *J. Am. Chem. Soc.*, 2025, **147**, 10992–10998.
33 W. Nowmann, *J. Chem. Phys.*, 2005, **123**, 064505.
34 S. Kim, J. Seo and S. Y. Park, *J. Photochem. Photobiol., A*, 2007, **191**, 19–24.
35 J. Wang, L. Lu, C. Wang, M. Wang, J. Ju, J. Zhu and T. Sun, *New J. Chem.*, 2020, **44**, 15426–15431.
36 J. Jiang, W. Lu, J. Cheng, L. Yang, H. Jiang, D. Bai and W. Liu, *Chem. Commun.*, 2012, **48**, 8371–8373.
37 *Date rape drug test allows women to discreetly check for spiked drinks with a few drops, Health and Science*, CNBC, 2018.
38 D. Zhai, B. K. Agarwala, P. F. S. Eng, S.-C. Lee, W. Xu and Y.-T. Chang, *Chem. Commun.*, 2013, **49**, 6170–6172.
39 D. Zhai, Y. Q. E. Tan, W. Xu and Y.-T. Chang, *Chem. Commun.*, 2014, **50**, 2904–2906.
40 S. D. Nuevalos, A. M. Costero, M. Parra, S. Gil, P. Arroyo, J. A. Saez, P. Gavina, P. Ceroni and A. Fermi, *Dyes Pigm.*, 2022, **207**, 110757.
41 S. D. Nuevalos, A. M. Costero, P. Arroyo, J. A. Saez, M. Parra, F. Sancenon and R.-M. Manez, *Chem. Commun.*, 2020, **56**, 12600–126003.
42 J. H. Contreras, J. R. Rubio, M. Parra, S. Gil, P. Arroyo, J. A. Saez, C. Lodeiro and P. Gavina, *Sens. Bio-Sens. Res.*, 2024, **46**, 100691.
43 S. Zhang, Y. Liu, J. Dong, J. Li, D. Lei and X. Dou, *Anal. Chem.*, 2024, **96**, 9026–9033.
44 R. Dahiwadkar, H. Kumar and S. Kanvah, *J. Photochem. Photobiol., A*, 2022, **427**, 113844.
45 D. Bokotial, P. Bhandari, M. Jaisawal, T. das, G. R. M. Rajendran, M. Mukherjee, S. Kyndait, G. Pramanik, S. Dasgupta and A. Chowdhury, *Chem. – Eur. J.*, 2025, **31**, e202500114.
46 D. Bokotial, S. Bhattacharyya, S. Arunkumar, T. das, G. R. M. Rajendran and A. Chowdhury, *Chem. – Eur. J.*, 2024, **30**, e202402086.
47 S. Bhattacharyya, A. Chowdhury, R. Saha and P. S. Mukherjee, *Inorg. Chem.*, 2019, **58**, 3968–3981.
48 W. Wang, Z.-Z. Dong, G. Yang, C.-H. Leung, S. Lin and D.-L. Ma, *J. Mater. Chem. B*, 2017, **5**, 2739–2742.
49 J. Ryu and Y. Kim, *Sens. Actuators, B*, 2022, **364**, 131861.
50 E. Garrido, G. H. Siguenza, E. Climent, M. D. Marcos, K. Rurack, P. Gavina, M. Parra, F. Sancenon, V. M. Centelles and R. M. Manez, *Sens. Actuators, B*, 2023, **377**, 133043.

51 J. H. Contreras, J. R. Rubio, M. Parra, S. Gill, P. Arroyo, J. A. Saez, C. Lodeiro and P. Gavina, *Microchim. Acta*, 2025, **192**, 275.
52 J. E. R. Moss, K. Hanmory, R. Moreland, C. B. Oakley, D. K. Bwambok and V. E. F. Narcisse, *Forensic Sci.*, 2025, **5**, 28.
53 M. Sharma, Shagun, A. Chillar, A. Jaisawal and A. Dhir, *Analyst*, 2025, **150**, 4597–4602.
54 M. Attia, *Spectrochim. Acta, Part A*, 2009, **74**, 972–976.
55 S. Chen, Y. Qiu, S. Yu, N. Ma, X. Zhang and J. Kong, *Spectrochim. Acta, Part A*, 2025, **326**, 125226.
56 A. Ghafarloo, R. R. Sabzi, N. Samadi and H. Hamisekhar, *J. Photochem. Photobiol., A*, 2020, **388**, 112197.
57 Y.-Y. Ten, Y.-S. Lin, T.-H. Chen, S.-C. Chyneh and H.-T. Chang, *Sens. Actuators, B*, 2020, **305**, 127441.
58 M. Abbasi, A. Jouyban, F. Ranjbar and J. Soleymani, *J. Mol. Recognit.*, 2024, **37**, e3088.
59 A. S. Maybodi, J. Abbasifar and M. Malekaneh, *Int. J. Pharm. Res.*, 2019, **21**, e127351.
60 T. Fan, W. Xu, J. Yao, Z. Jiao, Y. Fu, D. Zhu, Q. He, H. Cao and J. Cheng, *ACS Sens.*, 2016, **1**, 312–317.
61 K. Yan, L. Wang, H. Zhou, Z. Hua, P. Xu, H. Xu, Y. Wang, B. Di and C. Hu, *Dyes Pigm.*, 2022, **197**, 109875.
62 J. H. Contreras, P. Madrigal, P. Arroyo, M. L. Gonzalez, S. Gil, M. Parra, J. A. Saez and P. Gavina, *Dyes Pigm.*, 2024, **221**, 111806.
63 Y. Ding, X. Li, Y. Guo, J. Yan, J. Ling, W. Li, L. Lan, Y. Chang, J. Cai and L. Zha, *Anal. Bioanal. Chem.*, 2017, **409**, 7027–7034.
64 H. Chen, Y. Zhou, X. Jiang, F. Cao and W. Liu, *RSC Adv.*, 2019, **9**, 36884–36889.
65 M. A. Tantawy, M. A. Farag and A. M. Yehia, *New J. Chem.*, 2020, **44**, 7058–7064.
66 A. M. Yehia, M. A. Farag and M. A. Tantawy, *Anal. Chim. Acta*, 2020, **1104**, 95–104.